PHYSICAL REVIEW B VOLUME 48, NUMBER 10 1 SEPTEMBER 1993-II

Exchange coupling in magnetic heterostructures

M. D. Stiles
National Institute of Standards and Technology, Gaithersburg, Maryland 20899
(Received 3 May 1993)

Many structures consisting of magnetic layers separated by a nonmagnetic spacer layer show an oscillatory exchange coupling. This behavior is explained in terms of a simple model that shows that the Fermi surface of the spacer-layer material is responsible for the oscillatory coupling. The periods of the oscillatory coupling are set by extremal spanning vectors of the Fermi surface of the spacer-layer material. The strength of the coupling depends both on the geometry of the Fermi surface and on the reflection amplitudes for electrons scattering from the interfaces between the spacer layers and the magnetic layers. To test this and related models, the extremal spanning vectors and the associated Fermi-surface geometrical factors have been calculated for a large set of spacer-layer materials and interface orientations. These models are at least consistent with the experimental data. All measured oscillation periods are consistent with the calculated periods, but particularly for transition metals there are many more periods calculated than are seen experimentally.

I. INTRODUCTION

Since the discovery that magnetic films separated by a nonmagnetic spacer layer could be coupled antiferromagnetically,[1] and the subsequent discovery that the coupling could oscillate between ferromagnetic and antiferromagnetic,[2] there has been intense effort in understanding this phenomena. The interest is in part driven by the possible technological uses of these systems. When a system that is antiferromagnetically aligned is placed in a field large enough to reverse the magnetic alignment, there is a large change in the resistance of the system.[3,4] If the change in resistance can be made large enough while the field required to reverse the magnetizations is made small enough, these systems would be very sensitive detectors of magnetic fields. Small, sensitive detectors of magnetic fields have many possible applications,[5] including nonvolatile memory elements and read heads for magnetic data storage.

The coupling itself has been the subject of much experimental and theoretical interest, particularly with respect to the period of the oscillatory coupling. In all of the theoretical models, the periods are determined by properties of the Fermi surface of the spacer-layer materials. The periods measured on samples grown by molecular-beam epitaxy, Cr/Fe,[6–8] Mo/Fe,[9] Cu/Co,[10–13] Cu/Fe,[14,10,15] Ag/Fe,[16] Au/Fe,[17] Al/Fe,[17] Pd/Fe,[15] and Ru/Co (Ref. 18) agree well with the predictions of these theories.

In contrast, a common period is measured in most cases on samples grown by sputtering. For samples grown by sputtering with Co as the magnetic layers, seven systems, V,[19] Cu,[19–24] Mo,[19] Ru,[19,25] Rh,[19] Re,[19,26] and Ir,[19] have been found to have periods in the range 0.9–1.2 nm, while two systems, containing either Cr (Ref. 19) or Os (Ref. 27) have longer periods (1.8 nm and 1.5 nm, respectively). Other spacer-layer materials between Co layers have been investigated where either no coupling or no periodicity was found. Measurements of sputtered systems with Fe magnetic layers have found periods in the 0.9–1.2 range for Cu,[21] Nb,[28] and Mo,[29] but Cr (Ref. 2) (1.8 nm) is again the exception. The existence of a common period in such a variety of systems has led to speculation[19] that the oscillatory coupling has an origin that is independent of the Fermi surface of the spacer-layer materials.

This paper discusses a simple model that shows why the Fermi surface of the spacer layer plays an important role in the coupling between the magnetic layers in these systems. This model forms a framework to understand the theoretical treatments of the coupling. It shows that the periods expected in these theories are determined by extremal Fermi-surface spanning vectors. The coupling strengths are determined both by the geometrical properties of the Fermi surface, and by scattering properties of electrons reflecting from the interfaces between the two materials.

To test whether these models are consistent with the existing experimental data I compute the relevant extremal Fermi-surface spanning vectors of a large set of spacer-layer materials for several low index interface orientations. I find for metals with simple Fermi surfaces, like the noble metals, that there are only a few extremal spanning vectors, and that they are in good agreement with experimentally measured periods. On the other hand, for the transition metals, where the Fermi surfaces tend to be complicated, there are many extremal spanning vectors that could lead to a large variety of periods. Among these periods are some that agree with each of the periods that have been measured. The issue then becomes why are these periods and not others seen experimentally? Conclusive tests of these models require a detailed calculation of the coupling strengths for each of the possible periods, and a detailed analysis of what can

be inferred from the experimental data.

Section II of this paper presents a simple model for these metallic sandwich structures. Then I detail the calculation of the extremal spanning vectors for these materials. The results of the calculations are then compared with the existing experimental data. Finally, the simple model is compared with other theoretical treatments of the oscillatory coupling. A more detailed derivation of a general form for the oscillatory coupling and a derivation for the approximate results given in Sec. II are given in the Appendix.

II. MODEL

A one-dimensional quantum well is the simplest model that illustrates the oscillatory exchange coupling. Not only does it contain the essential physics by itself, but complications necessary to describe real systems can be added one at a time. The oscillatory exchange coupling arises because the energy that it takes to fill the electron states up to the Fermi level oscillates as a function of the well thickness. The period of the oscillation is given by the wave vector at the Fermi energy in the well. To understand this oscillatory energy, I consider first the states in the system, then the change in the density of states of the system with respect to the constituent materials, and finally the change in the total energy on filling the states to the Fermi level. From this starting point, I discuss the complications that arise in real systems due to the momentum parallel to the interface, general Fermi surfaces, and the underlying lattices.

This model is closely related to several that have been discussed previously. The discussion combines many aspects of these papers to motivate the numerical calculations that are discussed below. These previous contributions are discussed in Sec. V, where detailed referencing occurs.

A. Quantum-well states

To understand the states in the quantum well, first consider a single step; the material making up the well extends out to the left, and the material making up the asymptotic region extends to the right. The energy origin is chosen to be the band minimum in the asymptotic region. Thus, there is a threshold at $E = 0$ for states in the well material to be able to transmit across the step. At energies below threshold, a state incident from the left reflects with unit probability, and above threshold the reflection probability decreases from one to zero as the energy increases. This behavior is shown in Fig. 1(a).

When the second step is introduced, there are two types of states, bound states at negative energies, and scattering states at positive energies. At negative energies, a state reflects with probability one from each of the steps. In general the multiple reflections cancel each other and a state cannot exist. However, at discrete energies the interference is constructive and bound states result. These bound states consist of waves bouncing back and forth in the well with tails exponentially decaying into the asymptotic regions.

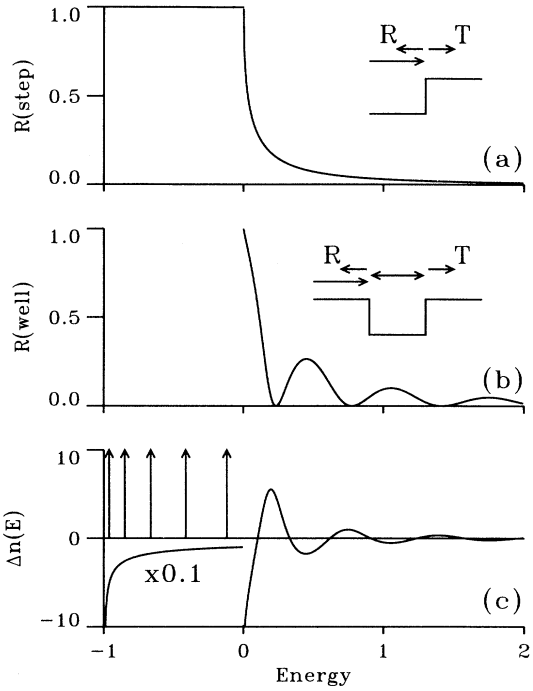

FIG. 1. Properties of a quantum well. (a) shows the probability for an electron incident from the well to reflect from a single step as a function of the energy. (b) shows the probability for an electron to reflect from the quantum-well structure. Insets in both panels schematize the processes. (c) shows the change in the density of states for the quantum-well structure. At negative energies, the curve has been reduced by a factor of 10 to fit it in the figure. The arrows represent the δ function contributions to the density of states due to the presence of bound states.

At positive energies there are scattering states at all energies. These scattering states consist of a plane wave incident on the quantum well from either side, a reflected wave with reduced amplitude on the same side of the well, waves scattering in both directions in the well, and a transmitted wave on the other side of the well. The probability for a state incident from either side to reflect from the well is shown in Fig. 1(b). The probability to transmit across the well is just one minus this probability. Since there are no states in the asymptotic regions with negative energies, the reflection probability is not defined for these energies. At low energies the reflection probability is one, decreasing to zero as the energy increases. However, unlike the reflection probability from a single step, the behavior as a function of energy is not monotonic.

The oscillatory component to the reflection probability is caused by transmission resonances. At energies close to those at which an integer number of wavelengths fit inside the well the state undergoes increased multiple scattering in the well, and transmits with unit probability. These resonances are closely related to the bound states of the potential. If the walls of the well were infinitely high, there would be bound states for positive energies. When the walls are not infinitely high, these positive en-

ergy bound states couple to the states in the asymptotic region and become resonances. Thus, the energies of the resonances follow the progression of the bound state energies. The widths of the resonances are determined by the coupling of the former bound states to the asymptotic region, which is determined by the reflection probability from a single step. When the step reflection probability is close to one, the resonances are narrow and as the reflection probability decreases the resonances broaden. This behavior can be seen by comparing the width of the resonances in Fig. 1(b) with the step reflection probability in Fig. 1(a).

The set of states consisting of the bound states, plus the scattering states incident from each side make up a complete set of states for this potential. The probability densities for several of these states are shown in Fig. 2. Shown in order of increasing energy are a bound state, a resonant scattering state, and a nonresonant scattering state. There is not a great difference between the probability densities for the resonant and the nonresonant states. The differences are due to the changing amount of interference between left and right going waves depending on the amount of reflection. They are small because the reflection probabilities for scattering from the steps are significantly less than at the energy of the resonance, and the resonances are broad. The changes in the probability densities lead in a complicated way to changes in the density of states.

The change in the density of states due to making a quantum-well structure has been investigated by inverse photoemission and photoemission.[30–34] The systems investigated were more complicated than the simple model discussed here because the spacer layer had magnetic material on one side and vacuum on the other. Still, the same general considerations hold; the system is a quantum well with one interface perfectly reflecting. For a variety of systems, the authors find peaks in the experimental spectra that disperse in energy as a function of the thickness of the overlayer. These peaks correspond to the peaks in the density of states discussed above. Interpreting the results in detail requires including many of the complications discussed below, including spin dependence, realistic band structures, and realistic calculation of reflection amplitudes from the interfaces.

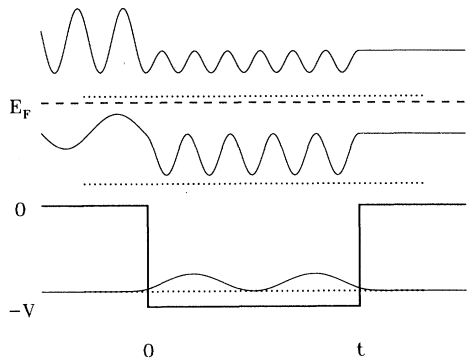

FIG. 2. One-dimensional quantum well and states. The heavy line shows the potential energy for a quantum-well structure. The dashed line gives the Fermi energy for the structure. The dotted lines are the energies at which states are shown and the thin lines are the probability densities for three states, in order of increasing energy, a bound state, a resonant scattering state, and a nonresonant scattering state.

B. Total energy of a quantum well

To compute the energy required to fill these states up to some Fermi level, it is necessary to compute the change in the density of states for this structure with respect to the constituent materials. Both the material making up the asymptotic region, material A, and the material making up the well, material W, have a density of states per unit length of $n_A(E)$ and $n_W(E)$, respectively. From these bulk densities of states, the change in the density of states for making a structure with a well thickness, t, and total asymptotic thickness, L, is

$$\Delta N(E,t,L) = N(E,t,L) - Ln_A(E) - tn_W(E). \quad (1)$$

In the limit that the size of the asymptotic region, L, goes to infinity, the change in density of states is independent of L. The rest of this discussion will consider this limiting quantity, $\Delta N(E,t)$.

This change in the density of states is shown for the quantum well of Fig. 2 in Fig. 1(c). At negative energies, where there are no states at most energies, there is a negative change in the density of states due to the loss of the states which were present in the bulk material. Since the bulk density of states is proportional to the square root of the energy, this negative contribution also behaves like the square root of the energy with respect to the potential minimum in the well. Superimposed on this negative density of states is a series of positive δ functions, one for each bound state. At positive energies, the transmission resonances give peaks in the change in density of states. In general, the density of states diverges like the square root of the energy at threshold, however, as is discussed below, this divergence can be either positive or negative.

The behavior of the change in density of states at positive energies can be understood in terms of the behavior at negative energies in much the same way that the transmission resonances can be understood in terms of bound states. First, the square root loss in the density of states is continued up to positive energies. Second, there are δ functions for the positive energy bound states superimposed on this loss. Finally the δ functions are broadened by the coupling with the continuum in the asymptotic regions. The overlapping broadened δ functions, superimposed on the negative background, then give the decaying oscillation that is seen in the change in the density of states.

To understand the change in the energy as a function of the well thickness, it is useful to examine the change in the density of states as a function of thickness, which is shown in Fig. 3. The lower part of the figure shows the evolution of the bound state energies as a function of the thickness. At a fixed energy, the bound states occur as a function of thickness with a separation of $\Delta t = 2\pi/2k_{\text{well}}$, where $\hbar k_{\text{well}} = \sqrt{2m(E+V)}$ is the wave vector of a state

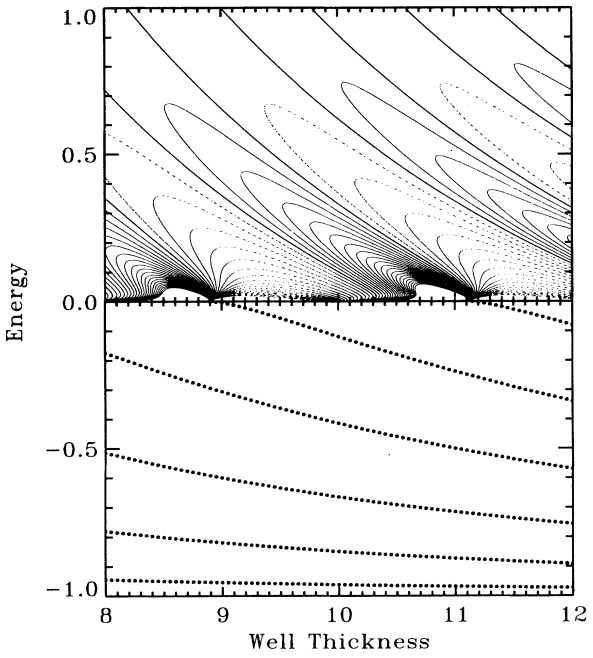

FIG. 3. Change in density of states for a quantum well. The top half of the figure is a contour plot of the change in the density of states as a function of energy and thickness of the quantum well. The contours are separated by 0.1 inverse energy units, and the dotted contours are negative. The bottom half of the figure shows the energies of the bound states as a function of the well thickness.

in the well at that energy. In particular, new bound states enter the well with a separation determined by the wave vector in the well at the energy of the threshold.

This spacing of the structure in the change in the density of states continues into the behavior for positive energies. At fixed energy, the resonances are separated by a thickness, $\Delta t = 2\pi/2k_{\text{well}}$. In, particular, this relationship holds true at the Fermi level. At high energies, the resonances are broad, so there are only weak oscillations in the density of states as a function of thickness. As energy decreases, the resonances become sharper and have a larger peak value due to the increasing single-step reflection probability. As they approach the threshold energy from above, they become infinitely sharp and change almost continuously into bound states. When a new bound state appears, the divergence in the density of states for positive energies changes sign from positive to negative.

Filling all the electron states in the structure up to the Fermi level gives the total electronic energy of the system. Then, subtracting the bulk energies of the constituent materials leaves the change in the energy due to making the well structure. This can be computed by first finding the change in the integral of the electron energies,

$$\Delta E_0(t) = \int_{-\infty}^{E_F} dE\, E\Delta n(E,t). \tag{2}$$

This is not the total change in the energy however. Simply integrating the change in the density of states also gives a nonzero result,

$$\Delta N(t) = \int_{-\infty}^{E_F} dE\, \Delta n(E,t). \tag{3}$$

If this change is positive, there is a net increase in the change of density of states at energies below the Fermi level and electrons have to be taken from the Fermi level to fill those states. If the change is negative electrons need to be added in at the Fermi level. Since the calculation is done in the limit that the asymptotic regions are infinitely big, there is an infinite density of states at the Fermi level, and the Fermi level itself does not change when a finite number of electrons are added or subtracted. Putting these two contributions together gives the total change in energy,

$$\Delta E(t) = \int_{-\infty}^{E_F} dE\, (E - E_F)\Delta n(E,t). \tag{4}$$

This change in the energy is shown in Fig. 4 as a function of the well thickness.

The dominant behavior of the change in energy as a function of thickness is a damped oscillation. The period of the oscillation is $2\pi/2k_F$, where k_F is the Fermi wave vector for the bulk material that makes up the well. It can be shown that if the single-step reflection probability is small, the change in the total energy for large separations is given by

$$E_\infty(t) = \frac{\hbar}{\pi}\frac{v_F}{2}|R_{\text{step}}|^2\frac{1}{t}\sin(2k_F t), \tag{5}$$

where $v_F = \hbar k_F/m$ is the electron velocity at the Fermi level, and $|R_{\text{step}}|^2$ is the reflection probability from a single step. The stronger the reflection, the stronger the oscillations in the density of states and the stronger the oscillation in the change in total energy. The falloff in the amplitude of the oscillation, $1/t$, only holds for large well thicknesses. For small thicknesses, other contributions are important, changing the effective period, and keeping the envelope from increasing without bound. The

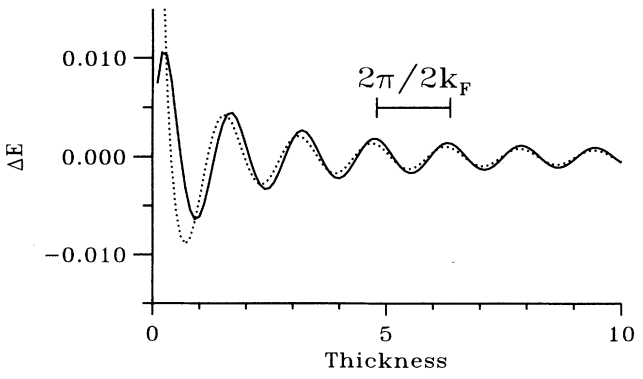

FIG. 4. Total energy of the quantum well filled to the Fermi level. The solid line shows the energy, calculated by filling states up to the Fermi level; the dotted line shows the asymptotic form, Eq. (5), for all thicknesses.

subscript on the energy $E_\infty(t)$ indicates that this behavior is exact only in the limit that the thickness of the well becomes large. However, as is seen in Fig. 4, this asymptotic form is quite accurate for thicknesses greater than one period. In general, the accuracy of the asymptotic form depends on the details of the band structures of the two materials, in particular on the strength of the reflection.

At this point, it is useful to note that the oscillations depend on a property of the bulk material that makes up the spacer layer, even though the spacer layer is not periodic throughout all space. This dependence on the bulk properties arises because the potential in the middle of the spacer layer is the same as it is in a bulk material, and hence, the electrons there respond as they would in a strictly bulk material. In this model, the potential is exactly the same by construction, while in real structures it is approximately correct. Since screening is very rapid in metals, this approximation is valid for all but the thinnest spacer layers. However, there are significant modifications in the potential close to the interfaces, which could lead to large changes in the reflection probabilities.

The oscillation as a function of distance with a period set by the Fermi surface is a general property of metals. Whenever a metal is subject to a spatially localized perturbation it responds with oscillations in the electron density with a period set by the Fermi surface. These density oscillations can also be manifest as spin density waves if the perturbation is spin dependent or as oscillatory energies between two different perturbations. Here, the perturbations are the boundaries with the magnetic material.

C. Exchange coupling

For magnetic sandwich structures the oscillatory exchange coupling arises for the same reasons as the oscillatory energy in a quantum well. However, it is much easier to detect because it is much easier to measure the magnetic state of a material than its total cohesive energy. In magnetic structures each spin system experiences a different potential. Model potentials for both spins are shown in Fig. 5 for the cases of ferromagnetic and antiferromagnetic alignment of the magnetizations. For each spin system the energy oscillates for the different magnetic configurations; the difference in these oscillatory energies is the oscillatory exchange coupling. There are three different oscillatory energies, one each for spin-up and spin-down electrons in a ferromagnetically aligned sample, and one for either spin in an antiferromagnetically aligned sample. All of the oscillatory energies have the same period because the period is determined by the Fermi surface of the bulk spacer-layer material, but since the potential barriers are different, the reflection probabilities are different, and hence the amplitudes of the oscillatory energies are different. Taking the difference between the sum of the energies for the spin-up and spin-down electrons in a ferromagnetically aligned sandwich and twice the energy for either spin in an antiferromagnetically aligned sandwich gives the exchange coupling,

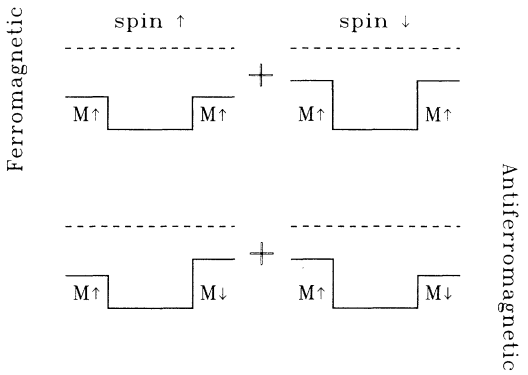

FIG. 5. Quantum wells for exchange coupling. The top left (right) quantum well shows the potential seen by spin-up (-down) electrons in a ferromagnetically aligned quantum-well structure. The bottom left (right) quantum well shows the potential seen by spin-up (-down) electrons in an antiferromagnetically aligned quantum-well structure.

$$J_\infty(t) = \frac{\hbar}{\pi}\frac{v_F}{2}\left[|R_\uparrow^\uparrow|^2 + |R_\downarrow^\uparrow|^2 - 2|R_\uparrow^\uparrow R_\downarrow^\uparrow|\right] \times \frac{1}{t}\sin(2k_F t + \phi_0), \tag{6}$$

where $R_\uparrow^\uparrow$ ($R_\downarrow^\uparrow$) is the reflection amplitude for a spin-up (-down) electron in the well material reflecting from an up magnetization barrier, and $R_\uparrow^\uparrow = R_\downarrow^\downarrow$ and $R_\downarrow^\uparrow = R_\uparrow^\downarrow$. Thus, the exchange coupling found in magnetic sandwich structures has the same origin as all other oscillation behavior in metals, the response of the electrons at the Fermi surface.

D. Parallel wave vectors

If the interfaces between the magnetic material and the nonmagnetic material are coherent, that is, the materials share a common lattice net, then the momentum parallel to the interface is conserved when an electron scatters from the interface. This is the case considered in the rest of the paper except for a brief discussion of disordered interfaces. Even if the interfaces are not coherent, understanding the behavior for coherent interfaces forms a good basis for understanding the behavior of disordered interfaces.

If parallel momentum is conserved, the problem breaks up into a set of one-dimensional models like the model discussed above. Each of these one-dimensional models contributes a component to the energy that oscillates in thickness with a period set by the Fermi-surface spanning vector for that parallel momentum. However, most of these different oscillations cancel out when all of the one-dimensional models are summed over. For a spherical Fermi surface the change in the energy per unit area of the interface is

$$\frac{E_\infty(t)}{A} = \int \frac{dk_x}{2\pi} \int \frac{dk_y}{2\pi} \frac{\hbar}{\pi} \frac{v_F}{2} |R_{\rm step}|^2 \frac{1}{t} \sin(2t\sqrt{k_F^2 - K^2})$$
$$\approx \frac{\hbar}{\pi} \frac{v_F}{2} |R_{\rm step}|^2 \frac{1}{t} \int \frac{dk_x}{2\pi} \int \frac{dk_y}{2\pi} \sin(2t\sqrt{k_F^2 - K^2})$$
$$= \frac{-\hbar}{2\pi^2} \frac{k_F}{2} \frac{v_F}{2} |R_{\rm step}|^2 \frac{1}{t^2} \left[\cos(2k_F t) - \frac{\sin(2k_F t)}{(2k_F t)}\right], \quad (7)$$

where $\sqrt{k_F^2 - K^2}$ is the Fermi-surface spanning vector as a function of the magnitude of the parallel wave vector, K. For simplicity, v_F and $|R_{\rm step}|^2$ are assumed to be independent of parallel momentum, $\mathbf{K}$; they are not, but this dependence does not affect the asymptotic result. The cancellations that occur in the integral in the second line of Eq. (7),

$$\int dk_x \int dk_y \sin(2\sqrt{k_F^2 - K^2}t)$$
$$= \frac{k_F}{2t} \left[\cos(2k_F t) - \frac{\sin(2k_F t)}{(2k_F t)}\right] \quad (8)$$

are illustrated in Fig. 6. Note that the integration over parallel momentum contributes an additional power of thickness, t, in the decay of the envelope, and a phase shift from a sine to a cosine in the asymptotic region. Also, there is preasymptotic behavior that modifies the effective period of the first oscillation, making it about 20% bigger than the asymptotic period. Finally, the peaks in the coupling do not come from the oscillations due to the parallel momentum of the extremum, but of parallel momentum close to it. This point is illustrated in Fig. 6 by the displacement of the peaks of the integral from the arrows marking the peaks due to the contribution from the extremum. However, for thicker and thicker layers, the parallel momenta that contribute to the peak in the integral move closer and closer to the extremum. This point will be important when discussing coupling due to extrema at high symmetry points in Sec. II F.

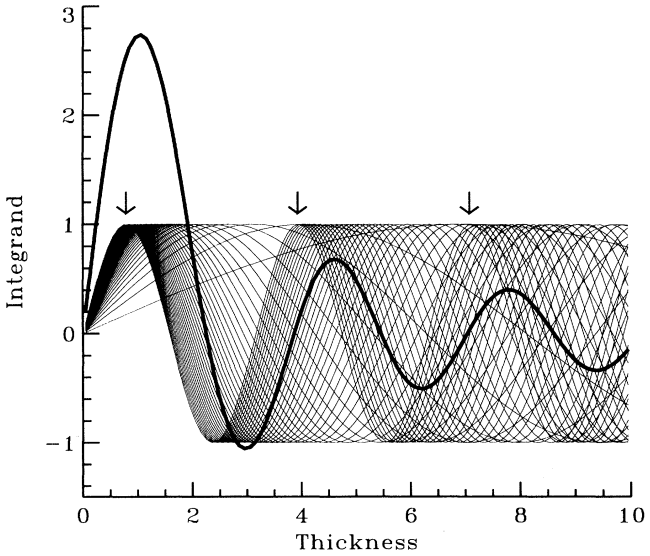

FIG. 6. Integration over parallel momentum. The integrand (20 thin lines) and result (heavy line) in Eq. (8) illustrate the cancellation of the the multiple oscillations in the integrand leaving only the oscillation due to the extrema. The arrows show the thicknesses of the peaks in the contribution from the extremum itself, rather than points close to it (see text).

E. General Fermi surfaces

For a nonspherical Fermi surface, the oscillatory coupling depends on the difference between two sheets of the Fermi surface. For the free-electron model discussed above, the two sheets are the two sides of the sphere. If the two sheets of the Fermi surface are $k_{Fi}(\mathbf{K})$ and $k_{Fj}(\mathbf{K})$, then the Fermi-surface spanning vectors are given by $\Delta k_{Fij}(\mathbf{K}) = k_{Fi}(\mathbf{K}) - k_{Fj}(\mathbf{K})$. The Fermi surface contributes an oscillatory term to the energy for each extremal spanning vector, defined by

$$\nabla_{\mathbf{K}} \Delta k_{Fij}(\mathbf{K})|_{\mathbf{K}_{\rm ext}} = \mathbf{0}. \quad (9)$$

There is a contribution whenever the spanning vector remains constant as the parallel momentum is changed.

Two geometrical factors contribute to the strength of the oscillatory energy, the curvature radius of the Fermi surface, and the reduced velocity at the Fermi surface. For a sphere the curvature radius of the difference of the two sheets is $k_F/2$; for the general shaped Fermi surface it is given by

$$\kappa_{ij} = \left[\sqrt{\frac{\partial^2 \Delta k_{Fij}(\mathbf{K})}{\partial k_x^2} \frac{\partial^2 \Delta k_{Fij}(\mathbf{K})}{\partial k_y^2} - \left(\frac{\partial^2 \Delta k_{Fij}(\mathbf{K})}{\partial k_x \partial k_y}\right)^2}\right]^{-1}. \quad (10)$$

There is only a contribution to the energy if the group velocities of the of the states at the Fermi surface for the extremal parallel momentum have opposite signs. If there are only two sheets of the Fermi surface this condition is always satisfied. The reduced Fermi velocity for the free-electron model is $v_F/2$; for a general dispersion this result generalizes to

$$v_{Fij}^{-1} = \left| \left(\frac{\partial E}{\partial k_z}\Big|_{\mathbf{k}=(\mathbf{K},k_{Fi})}\right)^{-1} - \left(\frac{\partial E}{\partial k_z}\Big|_{\mathbf{k}=(\mathbf{K},k_{Fj})}\right)^{-1} \right|. \quad (11)$$

Using these generalizations, the asymptotic oscillatory

contribution to the energy, Eq. (7), generalizes to

$$\frac{E_\infty(t)}{A} = -\left[\frac{\hbar}{2\pi^2}\kappa_{ij}v_{Fij}\right]|R_{ij}|^2\frac{1}{t^2}\sin(2k_Ft+\phi). \quad (12)$$

The phase change that comes about on integration over parallel momentum depends on the type of extrema, for a maximum $\phi = \pi/2$, for a minimum $\phi = -\pi/2$, and for a saddle point $\phi = 0$. The contribution to the exchange coupling from this extrema is then given by

$$\frac{J_\infty(t)}{A} = -\left[\frac{\hbar}{2\pi^2}\kappa_{ij}v_{Fij}\right]\left[|R_\uparrow^\uparrow|^2 + |R_\downarrow^\uparrow|^2 - 2|R_\uparrow^\uparrow R_\downarrow^\uparrow|\right] \times\frac{1}{t^2}\sin(2k_Ft+\phi). \quad (13)$$

A large oscillatory coupling requires a large geometrical weight, the first factor in square braces, and a large difference in the reflection amplitudes for the different configurations.

This simple form was presented by Edwards *et al.*[35] for the case where all reflection probabilities are either zero or one. A related form was derived from perturbation theory for planes of local moments by Bruno and Chappest.[36] The general form given above was previously presented by Bruno.[37]

The form for the oscillatory coupling, Eq. (13), only holds if there are only two sheets of the Fermi surface, and if all reflection probabilities are small compared to one. In spite of this qualifier, I use this result below to make comparisons between calculated extremal spanning vectors and measured oscillation periods. I calculate the extremal spanning vectors, and use the geometrical weights, the first quantity in square brackets in Eq. (13), as a guide to which extrema may be more important than others. However, the geometrical weight is only one contribution to the strength of the coupling and the other contributions may completely change the relative strengths of the couplings, so that this guide is not completely reliable.

A complete discussion of the coupling strength when more than one sheet is present, or when the reflection probabilities are not small compared to one is given in the Appendix, where general results are derived and the approximations necessary to find the above results are described.

F. Lattice effects

The above discussion has ignored the existence of an underlying lattice in the system. Some complications of having a lattice present are the existence of a reciprocal lattice, and, in turn, Brillouin zones. The existence of a lattice implies that there are infinitely many wave vectors that are equivalent to each other. An important consequence of this is that integrals over wave vectors need to be restricted to a finite region of reciprocal space to avoid overcounting the electron states. This finite region is called a Brillouin zone. While there is a standard choice for the Brillouin zone for each lattice, this choice is not unique, and for systems with interfaces another choice is more useful.

For all lattice vectors, $\{\mathbf{r}_0\}$, every point $\mathbf{r}$ is equivalent to the point $\mathbf{r}+\mathbf{r}_0$. Each lattice has a reciprocal lattice associated with it, $\{\mathbf{g}\}$, such that $\mathbf{r}_0\cdot\mathbf{g} = 2\pi n$, where n is some integer, for each $\mathbf{r}_0$ and $\mathbf{g}$. Every wave vector $\mathbf{k}$ is equivalent to $\mathbf{k}+\mathbf{g}$. The states associated with two wave vectors, $\mathbf{k}$ and $\mathbf{k}+\mathbf{g}$, are exactly the same states. Thus sums (integrations) over all states can only include the states associated with one of these wave vectors. Typically, this is done by restricting the integration to be over the region inside a Brillouin zone which includes each inequivalent wave vector exactly once. Usually, this zone is chosen to have the full point group symmetry of the lattice, but this is not necessary. The only requirement that a Brillouin zone need satisfy is that it fill space when translated by all of the reciprocal lattice vectors, $\{\mathbf{g}\}$. For situations in which there is a surface or an interface present it is more useful to choose a Brillouin zone that has the point group symmetry of the interface.

When electrons scatter from an interface between crystals with a common lattice net, momentum parallel to the interface is conserved, but momentum perpendicular to it is not. In this situation, it is useful to define a Brillouin zone such that all states that can couple to each other lie along a line through the chosen Brillouin zone. The obvious choice is a prism with a base determined by the interface Brillouin zone which is defined by the interface reciprocal lattice (discussed below). The height of these interface adapted bulk Brillouin zones is determined by the interlayer spacing, d.

The two-dimensional interface lattice vectors, $\{\mathbf{R}_0\}$, define an interface reciprocal lattice, $\{\mathbf{G}\}$, such that, $\mathbf{R}_0\cdot\mathbf{G} = 2\pi n$, where n is an integer, for all $\mathbf{R}_0$ and $\mathbf{G}$. Every two-dimensional wave vector $\mathbf{K}$ is equivalent to $\mathbf{K}+\mathbf{G}$ for all $\mathbf{G}$. The standard interface Brillouin zone includes only those parallel wave vectors such that $\mathbf{K}\cdot\mathbf{G} < \mathbf{G}\cdot\mathbf{G}/2$ for all $\mathbf{G}$. This interface Brillouin zone forms the base of the interface adapted bulk Brillouin zone. The height of the interface adapted bulk Brillouin zone is given by $2\pi/d$, where d is the interlayer spacing. Several of these interface adapted bulk Brillouin zones are shown in Fig. 7 for some low index interfaces for face-centered-cubic (fcc) and body-centered-cubic (bcc) lattices. In this figure, it is possible to see that the bulk Brillouin zone can be cut into pieces such that each piece can be translated by a reciprocal lattice vector to exactly reconstruct the interface adapted bulk Brillouin zone. This procedure illustrates the point that each Brillouin zone contains each unique wave vector exactly once.

Since parallel momentum is conserved, only states with the same parallel momentum are coupled, which implies that the wave vector for the coupling is always in the direction of the interface normal. Thus, the coupling between two states only depends on the difference in the momentum perpendicular to the interface, Δk_z. The layer separation, d, defines a one-dimensional reciprocal lattice, $2\pi n/d$, for all integers n. Thus, the coupling wave vector Δk_z is equivalent to $\Delta k_z + 2\pi n/d$, for all n. It is useful to restrict all coupling wave vectors to lie within the simplest one-dimensional Brillouin zone defined by $|\Delta k_z| < \pi/d$. Since the coupling can only be sampled on layer planes, thicknesses of ℓd, it is impos-

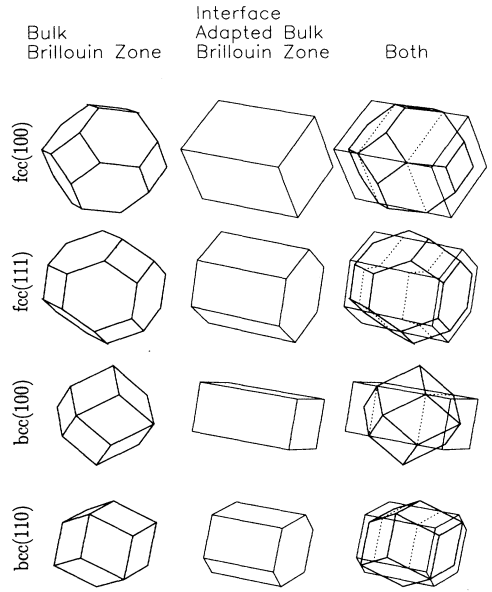

FIG. 7. Brillouin zones. The bulk Brillouin zones (left column) for face-centered-cubic (fcc) and body-centered-cubic (bcc) lattices (heavy lines) and interface adapted bulk Brillouin zones for several interfaces (center column) are shown superimposed (right column). The dotted lines show the intersections of planes from the two Brillouin zones. In the right column, both Brillouin zones are opaque for themselves, but transparent to each other.

sible to tell the difference between a coupling vector of Δk_z and $\Delta k_z + 2\pi n/d$ as $\exp[2\pi i \ell n(d/d)] = 1$. In the calculations I discuss in Sec. IV, all periods will be determined from wave vectors that have been shifted into this one-dimensional Brillouin zone.

Early on, mechanisms related to Ruderman-Kittel-Kasuya-Yosida (RKKY) exchange coupling were discounted because free-electron models predict oscillations with much shorter periods than are seen experimentally. It was pointed out that "aliasing"[35,38–40] could explain the observed periods. Aliasing comes about when a rapidly varying function (depending on the coupling wave vector) is sampled at well-separated discrete points (the lattice), and appears to be a slowing varying function (depending on the minimum of $|\Delta k_z + 2\pi n/d|$ for all n). While aliasing may seem like an artificial description in a free-electron model, in a real material the wave functions that determine the coupling are Bloch states, not simple plane waves. The Bloch states contain a whole series of wave vectors, differing only by reciprocal lattice vectors, and the resulting coupling should be described by the shortest wave vector component of the coupling.[41]

An additional complication compared to free-electron models is the calculation of the reflection probabilities for states scattering from the interface. For free-electron models it is possible to generate simple matching rules that give reflection probabilities that depend only on the band structures of the states. However, for realistic treatments of the electronic states, this is not possible because the reflection probabilities depend on the full atomic scale details of the wave functions. Not only is the strength of the reflection nontrivial, but there is also a phase change associated with the reflection that is not included in free-electron models.

One aspect of calculating realistic reflection probabilities is that states can have different symmetries along high symmetry lines in the Brillouin zone. If they do, they cannot couple. Thus, one might expect that extremal spanning vectors coupling states of different symmetry do not lead to an oscillatory coupling. However, this is not the case. For parallel wave vectors slightly displaced from the high symmetry line, the states can couple. As is discussed in Sec. II D, the peak contribution to the oscillatory coupling does not come from the extremum, but from states close to it. For larger and larger thicknesses of the spacer layer the important states are closer and closer to the extremum. So if the reflection probability goes to zero at the extremum, there is still an oscillatory coupling, but it falls off as a higher power of the thickness in the asymptotic region. However, larger thicknesses may be required before the asymptotic region is reached, and oscillatory couplings from states of different symmetry may still be important for experimentally relevant thicknesses. These considerations are important, because a large fraction of the extremal spanning vectors occur for high symmetry points.

One question raised by this model is how does the coupling strength depend on the thickness of the magnetic layers in a superlattice. At first glance one might expect this model to predict a similar dependence as found for the thickness of the spacer layer. A closer analysis shows that this is not the case. Even though there may be a strong oscillatory behavior to the energy of the magnetic layer as a function of thickness, it only depends weakly on the relative alignments of the magnetic layers, and largely cancels between the two alignments when computing the exchange coupling. The oscillatory exchange coupling, discussed above, arises from the difference in the reflection probabilities that electrons in the spacer layer see in the ferromagnetic and antiferromagnetic environments. In that case, the potential directly across the interface is different in the two cases. On the other hand, the electrons in the magnetic material see the same potential directly across the interface, just the spacer-layer potential. There is a difference in the two environments, but the electrons have to go all the way through the spacer layer before they detect this difference. Thus, the differences in the reflection probabilities between the two alignments is likely to be much smaller.

This entire discussion has ignored the fact that the charge oscillations that are set up by the standing wave states that give rise to the oscillatory coupling lead to a change in the potential that the electrons see. In principle, the whole calculation needs to be done self-consistently to take this change in the potential into account. On the other hand, when the spacer layer is thick, the changes in the potential more than a few layers from the interface are quite small, and do not have a significant effect on the exchange coupling. The changes in the layers close to the interface effectively just change the reflection probabilities, affecting the coupling strength, but

not the period of the oscillatory coupling. There are also constant shifts in the energy due to the charge rearrangement near the interface, but this largely cancels out in the exchange coupling.

III. METHOD

To test the model discussed above and related models, I have calculated the extremal Fermi-surface spanning vectors for a large set of possible spacer layers. First, I calculate the self-consistent electronic structure from a linearized-augmented-plane-wave (LAPW) implementation of the local density approximation (LDA). Then, I fit resulting band structures with a phenomenological tight binding approximation, which allows calculating the electronic structure on a much finer mesh in reciprocal space. Using this fit, I find the Fermi surface by one-dimensional searches as a function of parallel wave vector. I fit the Fermi surface locally to a quadratic function sheet by sheet. I find the difference between each pair of fit sheets and search for extremal spanning vectors. For each material, and each low index interface direction, I compile the set of extremal spanning vectors, and the associated geometrical weights. In the next section, Sec. IV, I discuss how the calculated extremal spanning vectors compare with experiment.

The LAPW electronic structure calculations were done for the bulk crystal structures as described elsewhere.[42] The plane-wave cutoffs for the the potential were 120 a_0^{-2} for face-centered-cubic (fcc), and body-centered-cubic structures (bcc), and 60 a_0^{-2} for hexagonal close-packed (hcp) structures. The plane-wave cutoffs for the wave functions were 15 a_0^{-2} for all structures. The final self-consistency iterations were done using 240, 408, and 108 special points in the irreducible wedge of the Brillouin zone for bcc, fcc, and hcp structures, respectively. The angular momentum cutoffs were $\ell = 8$ for bcc and fcc structures, and $\ell = 6$ for hcp structures. The cutoffs give electronic structures that are quite well converged.

The lowest lying bands for each structure were fit with a phenomenological tight binding model to speed up the calculation of the Fermi surfaces. The fitting procedure uses a three-center nonorthogonal parametrization including next-nearest neighbors for the fcc and bcc structures, and third neighbors for the hcp structures. This procedure uses 50, 60, and 164 fitting parameters for the bcc, fcc, and hcp structures respectively. It is similar to that described by Papaconstantopoulos[43] and is described elsewhere.[44] For the bands that cross the Fermi level, the quality of the fits range from a 2.4 meV root mean square (rms) error for Tc, to a 16.8 meV rms error for Al, with most fits being approximately 10 meV rms in error. Using the fit bands, the Fermi levels were found from a special points calculation using 5740 special points in the irreducible wedge of the Brillouin zone for fcc structures, 5200 special points for bcc structures, and 4200 special points for hcp structures.

The fit bands are used to find the Fermi surface for each material and interface orientation. For each parallel wave vector the points on the Fermi surface are found by bisection of some initial grid with additional bisections whenever a band is close to the Fermi level so that two points on the Fermi surface that are close to each are not missed. The points on the Fermi surface are collected into four-by-four sets of parallel wave vectors and sorted into sheets. Each of the sheets is least squares fit to a general quadratic form. By solving the least squares fit for an arbitrary set of data, the least squares fit is reduced to a matrix multiplication. The quadratic fits to each sheet are used to find extrema in the difference between each pair of sheets that have oppositely directed group velocities. At the same time the curvature of the extrema and the group velocities are found.

In the next section, the extrema are collected together and presented by the geometrical weight versus the period predicted by the extremal spanning vector and are compared with experiment. The geometrical weights are used as indicators of what the strength of the coupling associated with each extremal spanning vector might be. This indication is not that trustworthy; it has only been derived for regions of parallel wave vector where there is only one sheet of states moving in each direction, although it is physically reasonable that the same factors contribute in more complicated situations. Even for the simple situations, the coupling strengths still depend critically on the reflection probabilities for the states in the well, which can convert a large geometrical weight into a weak coupling strength or vice versa. Finally, even this form only holds asymptotically, and might be significantly modified for experimentally accessible layer spacings.

IV. COMPARISON WITH EXPERIMENT

Each spacer-layer material and each interface orientation has a set of extremal spanning vectors, and corresponding expected periods. These periods are compared to periods that are measured on samples grown by

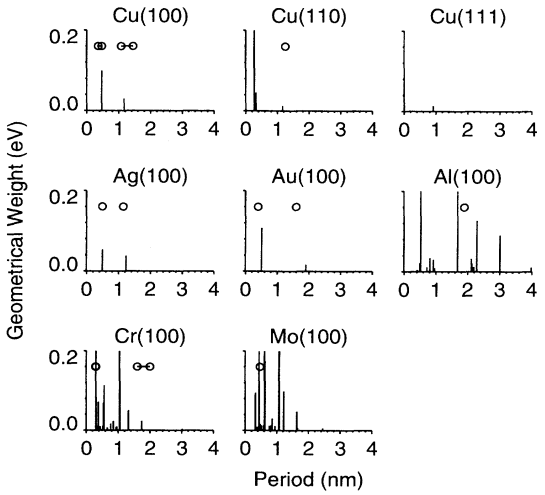

FIG. 8. Comparison between periods measured on samples grown by MBE and calculated extremal spanning vectors. The experimental data are shown as circles with an arbitrary y coordinate. The geometrical weight, see Eq. (12), for each extremal wave vector is plotted against the corresponding period.

molecular-beam epitaxy (MBE) in Fig. 8. The spanning vectors have been calculated assuming the bulk structure of the spacer-layer material. While the structure of the spacer layer is expected to be modified in many of the films, the modification is complicated, and for thick enough spacer layers, the structure should relax to the bulk structure. Only the periods are compared; the calculated geometrical weight is only included as a rough guide to which spanning vectors might be more important. In addition, the measured coupling strengths are more sensitive than the periods to the structural quality of the films, which can vary from system to system and from growth to growth. Below, I discuss the sources of uncertainty in both the calculation and the experiment.

The agreement for the noble metal interfaces is good. Ag(100) (Ref. 16) and Au(100) (Ref. 17) are closely lattice matched to Fe(100) when rotated by 45°, and can be grown reasonably well. For both, two periods are calculated and both are in good agreement with those that are measured. Cu(100) and fcc Co(100) are closely lattice matched and can be grown reasonably well;[10,12,13] Cu(100) and fcc Fe(100) structures can be grown with the Cu lattice constant if the Fe layers are kept thin.[14] For these systems the measurements are not as consistent. Short period and long period oscillations are found in one case.[10] In the other cases, long period oscillations are found, and in two of these cases the long period is significantly shorter than that found in the other measurements. The measured long periods bracket the calculated period. For the (110) interface between Cu and fcc Co the measured period[11] agrees well with the longest calculated period, and the shorter periods are not seen. For the (111) interface between Cu and either Co or fcc Fe the experimental results are still controversial.[11,45,46] Also, by appropriate choice of substrates, it is possible to force Cu into a bcc structure.[15,10] One measurement for (100) interfaces finds a short period oscillation, 0.36 nm,[10] and the other a long period oscillation, 1.4 nm.[15] The short period is consistent with spanning vectors calculated for a hypothetical bulk bcc Cu.[10]

For the other samples that have been grown by MBE the situation is more complicated. Al(100) (Ref. 17) and Cr(100)/Fe(100) (Refs. 6–8) are quite well lattice matched to Fe(100). For these systems there are many expected periods, only a few of which are seen experimentally. For Al, a long period is seen but the range of thicknesses investigated is not large enough to detect possible longer periods. While the lattice match is good, Fe and Al form many intermetallic compounds so that the interfaces are probably too rough for shorter period oscillations to survive. The situation is similar in Cr. When the growth is poor, a long period oscillation is observed, but when the growth is improved, a short period oscillation, layer-by-layer, is seen.[6] For good samples the short period oscillation is much stronger than the long period oscillation, and the former can mask the latter. The short period oscillations are clearly associated with the tendency toward antiferromagnetism in Cr. However, the short period oscillations are present to over twice the Néel temperature. These oscillations can be thought of in two equivalent ways. One way is to say that they are caused by the same Fermi-surface nesting as the antiferromagnetism. The other is to say that the Fe substrate stabilizes the antiferromagnetic state.

Several systems have been investigated that are not as well lattice matched. For Mo(100)/Fe(100),[9] a short period oscillation is observed, which is consistent with one of the many expected periods. For Ru(0001)/Co(0001),[18] a long period oscillation consistent with that found in samples grown by sputtering is found. For Pd(100)/Fe(100) (Ref. 15) oscillations are seen on a decaying antiferromagnetic background. The period is difficult to extract, but is consistent with a calculated period with a large geometrical weight. Short period oscillations have also been found for body-centered tetragonal Mn grown on Fe(100) (Ref. 47) which are consistent with the tendency of Mn toward antiferromagnetism as was the case for Cr.

There are many factors that complicate the comparison between calculated periods and measured periods. The main difficulty with the calculation is that the coupling strengths are not calculated, so that it is not known which possible periods are actually important. An additional source of error is the use of the local density approximation (LDA) to determine the Fermi surfaces. While LDA Fermi surfaces are found to be quite good, there is no rigorous justification for this, and hence no good estimate of the uncertainty. For some metals, high quality fits to the Fermi surface based on de Hass-van Alphen measurements can provide more reliable Fermi surfaces and extremal spanning vectors.[36]

There are several difficulties facing the experimental determinations of the periods. One difficulty is the roughness of the interfaces. Not only does this roughness wash out short period oscillations in a fairly straightforward way,[48] but it also changes coupling strengths in more basic ways.[49] Roughness breaks parallel momentum conservation at the interfaces, which can drastically effect the reflection probabilities that determine the coupling strength. Other difficulties are associated with the range of the measurement. If the range of thicknesses investigated is restricted, it is impossible to find periods longer than a certain amount. This difficulty is compounded by the decay of the oscillations, particularly when there may be several oscillations that decay differently. Additionally, as discussed above, the effective period measured at short separations may be different than the asymptotic period that would be measured for larger thicknesses. This is particularly so if the first antiferromagnetic peak is used in the determination of the period because the small thickness part of that peak may be strongly affected by the presence of pinholes in the spacer layer. Finally, a rigorous extraction of periodicities from the existing experimental data is quite difficult and in general ambiguous. Many more periodicities may be present in the data than have been extracted.

A set of experiments has been done on samples grown by sputter deposition. The results for these experiments with Co magnetic layers, V,[19] Cu,[19–24] Mo,[19] Ru,[19,25] Rh,[19] Re,[19,26] Ir,[19] Cr,[19] and Os (Ref. 27) are compared with calculated periods in Fig. 9. The structure of these samples is not as well known as the structure of the sam-

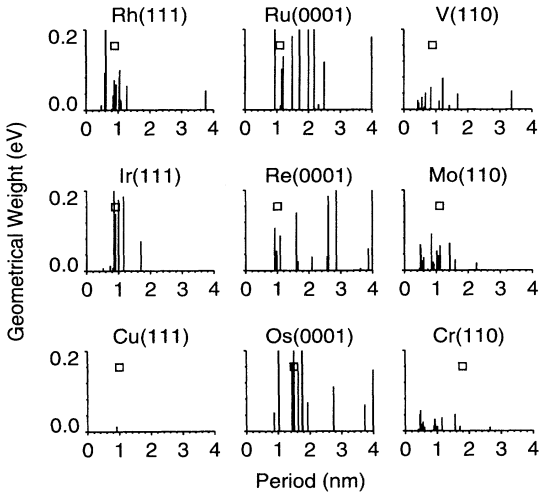

FIG. 9. Comparison between periods measured on samples grown by sputtering and calculated extremal spanning vectors. The experimental data are shown as squares with an arbitrary y coordinate. The geometrical weight, see Eq. (12), for each extremal wave vector is plotted against the corresponding period. For the calculations, the interface orientations are assumed to be the hexagonal or pseudohexagonal interfaces for the different bulk lattices.

ples grown by MBE. Since the samples were grown on Co(0001) substrates, I assume for the purpose of comparison that the dominant interfaces in these samples involve the hexagonal, fcc(111) and hcp(0001), or pseudohexagonal interfaces, bcc(110). For most of the samples at least, these were the strongest orientations found for the textured films in x-ray measurements.[19] As was the case for the samples grown by MBE, all of the measured periods are consistent with calculated periods. For many of these interfaces, almost any measured period would be consistent with a calculated period. Which of the periods are actually important has to wait for more detailed calculations.

An important issue is why seven out of the nine spacer layers have roughly the same period, 0.9–1.25 nm, Cr with a period of 1.8 nm and Os with a period of 1.5 nm being the exceptions. I argue that the explanation depends on the structure of the films and the nature of the measurement. As mentioned above, rough interfaces wash out short period oscillations, adding a short period cutoff to the experimentally observable periods. Measurement over a finite range adds a long period cutoff to the observable periods, because a long period oscillation may not be observable when superimposed on another decaying oscillation. A possible explanation is that periods close to 1.0 nm are seen because shorter and longer periods are filtered out.

While certainly true in part, this explanation is not complete, because in different films periods ranging from 0.8 nm to 1.8 nm have been observed. If this is the range of experimental sensitivity, more than one period might be expected for some of the films. Disentangling this issue requires both theoretical effort and experimental analysis. Both detailed calculations of the coupling strengths due to each extrema are necessary, and so are calculations of how they add to produce a final result. A superposition of many oscillatory components may give results that look periodic over a short range, but not if measured over a wider range. The experimental data would best be analyzed for the significance of the periods that are extracted. Ideally, this analysis should include estimations for the largest strength for couplings of a given period that can be ruled out by a given set of data.

Figures 10–15 show slices through the Brillouin zones relevant to the interfaces discussed above, indicating some of the important extremal spanning vectors. For the noble metals in the [100] direction, shown in Fig. 10, all of the slices look quite similar. They are free-electron-like with necks in the [111] directions and bulges in the [100] direction of the Brillouin zone. The long period oscillation is due to the free-electron-like spanning vector at the zone center, and the short period oscillation is due to the other spanning vector. For these interfaces, all of the inequivalent extremal spanning vectors can be seen in this figure. Since the free-electron sphere for Al extends into the third Brillouin zone, the Fermi surface is much more complicated than those of the noble metals. There are many extremal spanning vectors, only some of which can be seen in this figure. The free-electron-like extremal spanning vector at the zone center agrees well with the experimentally measured period.

For the the [111] direction in Cu, shown in the top of Fig. 11, there is no free-electron-like spanning vector because of the necks in the [111] direction. The only extremal spanning vector for this interface is seen at the zone boundary in this figure. For the (110) interface, shown in the bottom of Fig. 11, there are several extremal spanning vectors, only some of which are seen in this slice. The free-electron-like spanning vector at the zone center would give a short period oscillation that has not

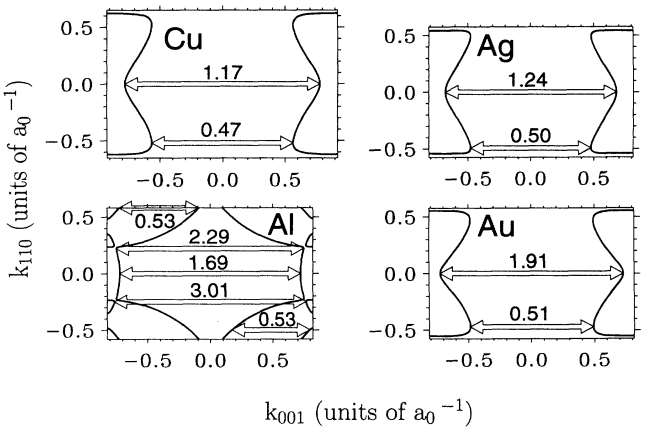

FIG. 10. Extremal spanning vectors for fcc(100) interfaces. Slices though the Fermi surface (heavy lines) in the interface adapted bulk Brillouin zone are shown for the noble metals and Al. Selected extremal spanning vectors (arrows) are labeled by the period in nm that would arise from the coupling of these parts of the Fermi surface. Note that some of the displayed spanning vectors are outside the one-dimensional Brilloun zone for coupling vectors and are translated back in before computing the period (see Sec. II F).

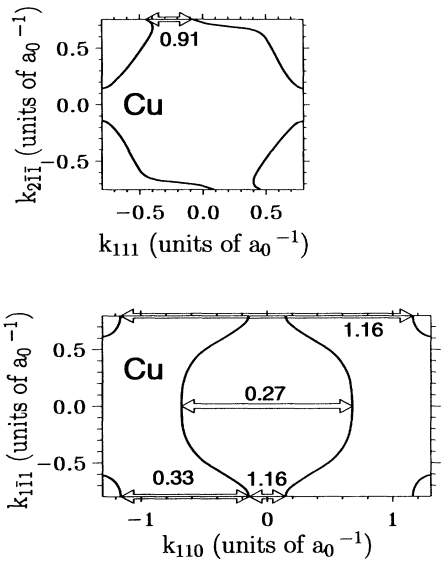

FIG. 11. Extremal spanning vectors for Cu(110) and Cu(111) interfaces. (Same as Fig. 10.)

been seen experimentally. The spanning vector at the neck gives a long period oscillation that is consistent with what is seen experimentally.

For (001) interfaces of Mo and Cr, shown in Fig. 12, there are large sections of the Fermi surface that are very nearly parallel, a condition called nesting, that give rise to the short period oscillations seen in these materials when grown by MBE. For Cr, there is an extremal spanning vector that gives a period of 1.74 nm, which is quite close to the long periods seen for Cr. A complication is that the two states that are coupled have different symmetry. Thus the coupling at the extremum is zero. However, as discussed above, this does not mean that there is no coupling with this period, just that the coupling falls off as a larger power of the thickness in the asymptotic region. Detailed calculations are needed to answer the question of whether the coupling from this spanning vector is strong enough to explain the experimental data.

Figure 13, Fig. 14, and Fig. 15 show slices through bcc,

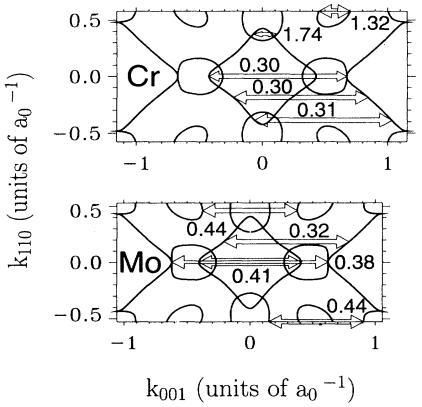

FIG. 12. Extremal spanning vectors for bcc(001) interfaces. (Same as Fig. 10.)

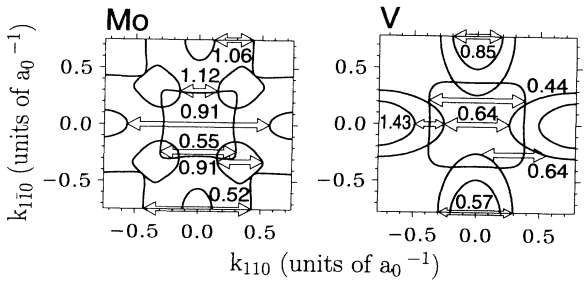

FIG. 13. Extremal spanning vectors for bcc(110) interfaces. (Same as Fig. 10.)

fcc, and hcp Brillouin zones, respectively. These slices are all relevant for interfaces in the comparison between calculated and measured periods shown in Fig. 9. In some cases, Rh(111) being a good example, the extremal spanning vectors close to the experimental value with the largest geometrical weights were at arbitrary points in the Brillouin zone, and not easily shown in a Brillouin zone slice. One interesting point is the difference in the Fermi surfaces for Ru and Os, which are very similar except for the small ellipse near the zone center for Ru. The extremal spanning vector for this small ellipse is close to the experimental period. The lack of this piece in the Fermi surface of Os may explain why the longer period is found there.

A collection of the extremal spanning vectors for a set of interface directions is given in Figs. 16–19. For each material, the extremal spanning vectors in three low index interface directions are shown. For most transition metals there are many periods in each direction, so that lacking a complete calculation of the coupling strengths, just about any period might be expected.

V. COMPARISON WITH OTHER MODELS

In some sense, calculations of the oscillatory exchange coupling can be described as different approximations for the reflection probabilities. While some models are based on simplified band structures, all give periods that are derived from extremal Fermi-surface spanning vectors for the Fermi surface they use. Thus, the only difference between the models is the approximations for the reflection

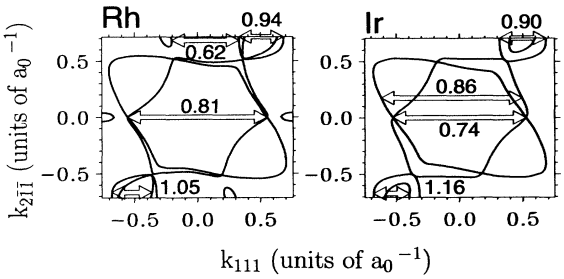

FIG. 14. Extremal spanning vectors for fcc(111) interfaces. (Same as Fig. 10.)

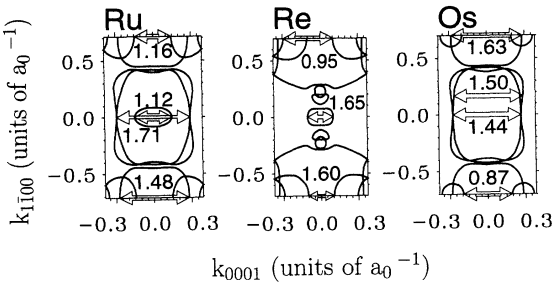

FIG. 15. Extremal spanning vectors for hcp(0001) interfaces. (Same as Fig. 10.)

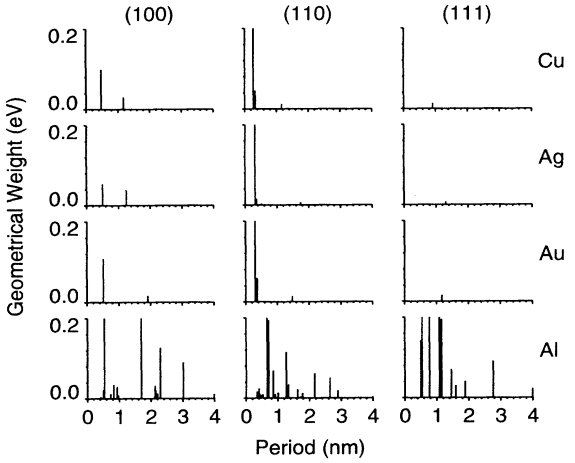

FIG. 16. Calculated extremal spanning vectors for noble metals and Al. The geometrical weight, see Eq. (12), for each extremal wave vector is plotted against the corresponding period for several interface orientations.

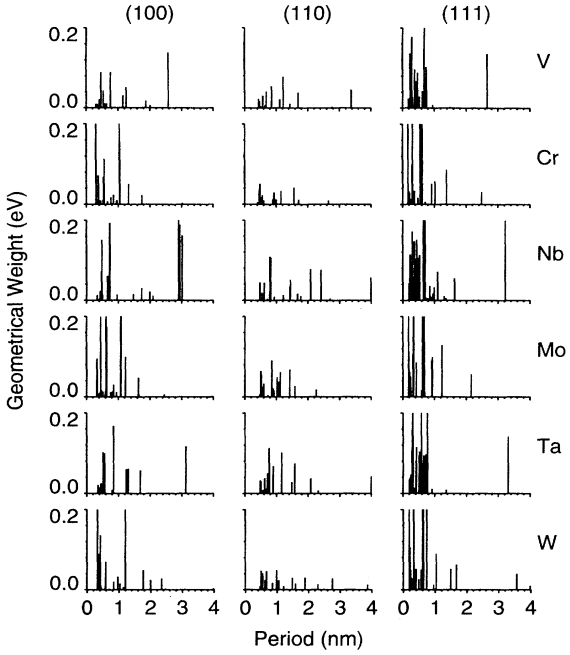

FIG. 18. Calculated extremal spanning vectors for several bcc transition metals. (Same as Fig. 16.)

probabilities. The calculated coupling strengths are only as good as these approximations. Even though the calculated coupling strengths are only approximate, these models have made important contributions to the understanding of the oscillatory coupling. Many of the calculations are reviewed in more detail in a review article by Hathaway.[50] Below, I discuss various calculations in terms of the approximations made for the reflection probabilities.

The discussion in Sec. II is very similar to that presented by Bruno.[37] His presentation is cast in terms of the single electron Green functions of a quantum well.

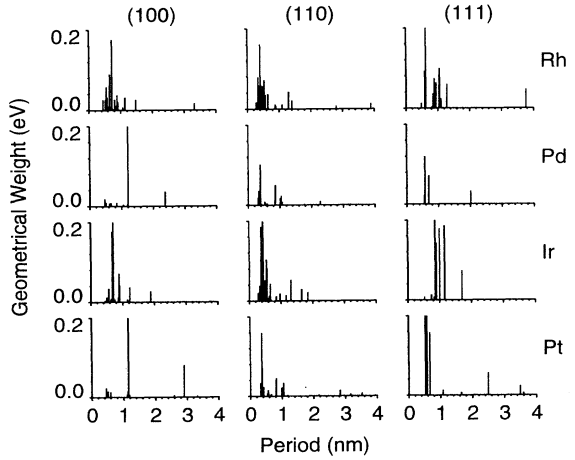

FIG. 17. Calculated extremal spanning vectors for several fcc transition metals. (Same as Fig. 16.)

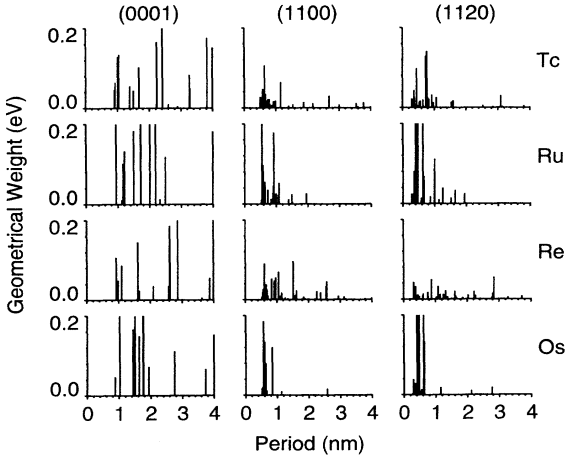

FIG. 19. Calculated extremal spanning vectors for several hcp transition metals. (Same as Fig. 16.)

While it may not be obvious, these Green functions contain exactly the same information as the reflection probabilities discussed above. These Green functions are a way of organizing the algebra. As I have done in this paper, he derives an expression for the exchange coupling in terms of reflection probabilities, but does not calculate them.

The specific calculation in terms of matching free-electron wave functions in a quantum well is identical to the calculation of Barnas[51] and those of Erickson, Hathaway, and Cullen[52–54] for the cases of ferromagnetic and antiferromagnetic alignments. Again, the latter calculations may appear different because their calculation is done in terms of a spin current as a function of energy rather than a change in density of states as a function of energy as is done here, but the two calculations are formally identical, and give the same result. In these calculations, the band structures of the transition metals are treated in a free-electron approximation, and the reflection probabilities are determined by matching free-electron wave functions at the interfaces between the materials.

In the calculation of Erickson *et al.*, the authors solve for the coupling for an arbitrary alignment of the magnetizations and show that there is not only a Heisenberg term like that discussed here, but also terms that are proportional to higher powers of the dot product of the two magnetization vectors, including the next term, which is one contribution to the biquadratic coupling.

The calculations of Edwards *et al.*[35,55–59] are also closely related to the previous model, and the one discussed in this paper. The main difference is that these authors use a tight binding band structure rather than a free-electron band structure. They omit the *s-p* bands and only include the bands derived from the *d* electrons. They also use the same bands in the antiferromagnetic material as in the ferromagnetic material but include an exchange splitting in the ferromagnet. In these calculations, the reflection probabilities are determined by matching the tight binding wave functions at the interfaces between the materials.

Edwards *et al.* have carried out a detailed study of the numerical integration over the parallel wave vector. They find that for large separations that an enormous number of parallel wave vectors are required. This requirement is not surprising because for large spacer-layer thicknesses the areas in parallel wave vector space that contribute to the oscillatory coupling are quite small. The "effective area" associated with each point in the numerical integration has to be much smaller than the area contributing to the oscillatory coupling. This fact will make convergence of first principles calculations quite difficult.

Deaven *et al.*[38] have studied a model Hamiltonian in which the the electrons are free parallel to the interface, but tight-binding-like perpendicular to it. They include nearest-neighbor exchange in the magnetic layer in a Hartree-Fock approximation. This simple model allows them to compare their nonperturbative calculations with perturbative calculations related to the Ruderman-Kittel-Kasuya-Yosida (RKKY) coupling between magnetic impurities in a nonmagnetic matrix. They find that the agreement between the two is quite good over the range of parameters they investigated.

Several authors, Lacroix *et al.*,[60,61] Levy *et al.*,[48,62–64] and Bruno and Chappert[40,47,65,66] have carried out perturbative, RKKY-like, calculations of the coupling strength. While the connection between these calculations and the description of the coupling in terms of reflection probabilites is less direct, it does exist. It is possible to think of a perturbative calculation of the scattering states in this geometry. The scattering states include the reflection probabilities, and can be used to calculate the change in the energy due to the perturbation. If such a calculation were carried out, and all terms of the appropriate order in perturbation theory were kept, the results would be exactly the same as a perturbative calculation of the energy. In this sense, these RKKY-like theories can be described as being based on a perturbative calculation of the reflection probability. The approximation for the reflection probabilities is then of free-electron-like states scattering from local moments.

Several calculations have been carried out for superlattices based on tight binding descriptions of the bands.[49,67–69] These calculations are a reasonable balance between effort and accuracy and can lead to considerable insight. They do have two drawbacks however: the tight binding parameters at the interface are not known, and very fine meshes are required in reciprocal space integrations. In these calculations the reflection probabilities depend on both the band structures of the materials, and also the matching rules that are used at the interface between the materials. Since the tight binding parameters for the interface are not known, the reflection probabilities used in such calculations are approximate. The calculations are complicated by the fact that they do not take advantage of the fact that the interior layers of the spacer layer are essentially the same. The consequence of this is that the calculations need to be done on an extremely fine mesh in the three-dimensional reciprocal space to be adequately converged, particularly for large spacer-layer thicknesses. The work of Stoeffler and Gautier[49,67,68] is based on a real space technique. While the connection with reciprocal space integrations may not be obvious, the requirement of a fine mesh in reciprocal space translates into the requirement of very large real space calculations.

Finally, several fully self-consistent electronic structure calculations[70–75] have been carried out. While these calculations should give the correct answer if carried to convergence, they are extremely difficult to converge for the same reasons as the tight binding calculations. However, these are the only calculations that can realistically describe the reflection probabilities at the interfaces.

Except for the self-consistent electronic structure calculations, none of the calculations described above can be expected to give accurate coupling strengths because they all are based on approximations for the reflection probabilities. On the other hand, the electronic structure calculations cannot be converged in the asymptotic region. An ideal calculation would take reflection probabilities calculated from first principles and use them in an approximate calculation that takes advantage of the

approximate symmetry of the interior layers in the spacer layer.

VI. SUMMARY

This paper has presented a simple model to show why Fermi-surface effects are expected to lead to oscillatory exchange coupling in metallic heterostructures. Complications were added to this simple model to make it relevant for realistic systems. The model shows that the periods of the oscillatory coupling are set by extremal spanning vectors of the Fermi surface of the spacer-layer material. The strength of the coupling depends both on the geometry of the Fermi surface and on the reflection amplitudes for electrons scattering from the interfaces between the spacer layers and the magnetic layers.

I have calculated the extremal spanning vectors and the associated Fermi-surface geometrical factors for a large set of spacer-layer materials and interface orientations. All measured oscillation periods are consistent with the calculated periods, but particularly for transition metals there are many more periods calculated than are seen experimentally. More work needs to be done before a quantitative comparison between theory and experiment is possible. Accurate calculations of the coupling strengths need to be carried out, and a more detailed analysis of the experimental data needs to be done.

Most models for the oscillatory coupling predict the same periods if they use the same band structure for the spacer-layer material. On the other hand, the calculations of the oscillatory coupling strength is still approximate. Most models make drastic approximations for the reflection probabilities, so that coupling strengths are correspondingly approximate. Self-consistent electronic structure calculations do not make these drastic approximations, but are very difficult to converge, even for extremely thin layers.

ACKNOWLEDGMENTS

I would like to thank R. J. Celotta, D. T. Pierce, J. Unguris, and W. E. Egelhoff for many stimulating conversations.

APPENDIX: GENERAL DERIVATION

In this appendix I derive the results presented in Sec. II. First, I discuss scattering states for an interface between materials with general band structures. From the properties of the scattering states I derive the form for the change in the density of states for such interfaces. Then, I show how this result reduces to the result given in Sec. II for the simple case where there is only one band crossing the Fermi surface. Finally I use the change in the density of states for the single-band case to derive the oscillatory energy of a quantum well in this situation.

1. Scattering states for general band structures

Reflection and transmission matrices for the scattering states have superscripts, which indicate, in order, the material on the left, the material on the right, and the direction of the incident state; thus $R^{\mathrm{I,II},R}$ is the reflection matrix for an interface between material I on the left, material II on the right, and a state incident from the left in material I, moving right toward material II. In region I (II) there are N_{I} (N_{II}) right moving states and N_{I} (N_{II}) left moving states. In terms of these states, a scattering state has the following form in the asymptotic region away from the interface:

$$\psi_{\mathrm{I},n} = \begin{cases} e^{ik_{\mathrm{I},R,n}x} u_{n_{\mathrm{I},R,n}}(k_{\mathrm{I},R,n}, x) + \sum_{m=1}^{N_{\mathrm{I}}} R^{\mathrm{I,II},R}_{n,m} e^{ik_{\mathrm{I},L,m}x} u_{n_{\mathrm{I},L,m}}(k_{\mathrm{I},L,m}, x), & x \ll 0 \\ \sum_{m=1}^{N_{\mathrm{II}}} T^{\mathrm{I,II},R}_{n,m} e^{ik_{\mathrm{II},R,m}x} u_{n_{\mathrm{II},R,m}}(k_{\mathrm{II},R,m}, x), & x \gg 0 \end{cases}$$

$$\psi_{\mathrm{II},n} = \begin{cases} e^{ik_{\mathrm{II},L,n}x} u_{n_{\mathrm{II},L,n}}(k_{\mathrm{II},L,n}, x) + \sum_{m=1}^{N_{\mathrm{II}}} R^{\mathrm{I,II},L}_{n,m} e^{ik_{\mathrm{II},R,m}x} u_{n_{\mathrm{II},R,m}}(k_{\mathrm{II},R,m}, x), & x \gg 0 \\ \sum_{m=1}^{N_{\mathrm{I}}} T^{\mathrm{I,II},L}_{n,m} e^{ik_{\mathrm{I},L,m}x} u_{n_{\mathrm{I},L,m}}(k_{\mathrm{I},L,m}, x), & x \ll 0, \end{cases} \tag{A1}$$

where the sum over m is a sum over all of the outgoing states at a given energy and parallel wave vector, and there is a state for each n representing an incoming state in each material. The parallel momentum dependence of the states has been suppressed for clarity. Close to the interface there are evanescent contributions to the wave functions that fall off away from the interface. If two interfaces are close to each other these contributions can become quite important, but they are ignored for the rest of the derivation. From here on, the Bloch functions, $u_n(k, x)$, are also suppressed.

The reflection and transmission amplitudes can be put

into matrix form in the obvious way giving matrices of the form

$$\begin{aligned} \text{Shape}[R^{\text{I,II},R}] &= N_{\text{I}} \times N_{\text{I}}, \\ \text{Shape}[T^{\text{I,II},R}] &= N_{\text{I}} \times N_{\text{II}}, \\ \text{Shape}[R^{\text{I,II},L}] &= N_{\text{II}} \times N_{\text{II}}, \\ \text{Shape}[T^{\text{I,II},L}] &= N_{\text{II}} \times N_{\text{I}}. \end{aligned} \tag{A2}$$

These matrices can in turn be made in to one large matrix:

$$S = \begin{pmatrix} T^{\text{I,II},R} & R^{\text{I,II},R} \\ R^{\text{I,II},L} & T^{\text{I,II},L} \end{pmatrix}. \tag{A3}$$

This matrix converts incoming states to outgoing states. If materials I and II are the same, with some arbitrary interface between them, the incoming Bloch states are the same as the outgoing Bloch states. In this case, all of the eigenvalues of S are phases. If this were not the case there would be amplification on going through the well, which violates flux conservation. In general, multiplying S on the left and right by the appropriate diagonal matrices containing the square roots of the group velocities for the Bloch states gives a unitary matrix.

2. Change in the density of states

The reflection and transmission matrices for a quantum-well structure with two interfaces can be built up from the reflection and transmission matrices for single interfaces. Such a calculation is based on the approximation that the evanescent parts of the wave function due to scattering from each interface do not affect the scattering from the other interface. The easiest way to carry out this calculation is to consider sequential multiple scattering processes and add amplitudes rather than solve the whole problem at once. This is possible because the Schrödinger equation is linear. Consider a situation with material I to the left of $-t/2$ and to the right of $t/2$ and material II in the middle. Consider some combination of possible incident states traveling from the left incident on the left interface. Part of the wave reflects with amplitudes given by the matrix multiplication of the reflection matrix times the array of the initial amplitudes and some transmits with amplitudes given by a similar matrix multiplication. The part that transmits traverses the well, region II, accumulating phase due to its propagation. The accumulation of phase can be accounted for by multiplying by a phase propagation matrix

$$\Phi^{\text{II},R}_{n,m,x} = \delta_{n,m} e^{ik_{\text{II},R,n}x}. \tag{A4}$$

Obvious generalizations of the matrix exist for right and left going states in both materials. When the transmitted wave reaches the other interface on the right, part of it transmits and part of it reflects. This process continues forever. There is some part of the wave that keeps reflecting off of the interfaces of the well, each time adding either to the amplitude to transmit through the structure or to the amplitude to reflect from it. The amplitude for each part of the process is given by successive matrix multiplications. Finally, all of the partial amplitudes are summed to give the transmission and reflection amplitudes for the well as a whole.

Fortunately after two round trips of multiple reflections in the well, the general form of all of the multiple scattering can be guessed and summed in closed form. The resulting reflection amplitude is

$$\begin{aligned} R^{W,R} = {} & R^{\text{I,II},R} \\ & + T^{\text{I,II},R}\Phi^{\text{II},R}_{t} R^{\text{II,I},R}\Phi^{\text{II},L}_{-t} \\ & \times \left[I - R^{\text{I,II},L}\Phi^{\text{II},R}_{t} R^{\text{II,I},R}\Phi^{\text{II},L}_{-t} \right]^{-1} T^{\text{I,II},L}, \end{aligned} \tag{A5}$$

and the transmission amplitude is

$$\begin{aligned} T^{W,R} = {} & T^{\text{I,II},R}\Phi^{\text{II},R}_{t} \\ & \times \left[I - R^{\text{II,I},R}\Phi^{\text{II},L}_{-t} R^{\text{I,II},L}\Phi^{\text{II},R}_{t} \right]^{-1} T^{\text{II,I},R}. \end{aligned} \tag{A6}$$

The transmission and reflection amplitudes for states incident from the right and moving to the left can be found in the same way and have the same form as these amplitudes. The inverse matrix in these expressions is due to the multiple reflection in the well.

The scattering states for the well structure form a complete set of states for each energy and parallel wave vector. The change in the density of states due to the presence of the well can be found from these results. Because the asymptotic parts of the structure are infinite in extent, the density of states is also infinite. Thus, the change in the density of states requires subtracting the infinite density of states of the "bare" constituent materials from the density of states of the well structure. To do this subtraction, consider a finite asymptotic region with periodic boundary conditions and take the limit that the size of the asymptotic region, L, goes to infinity. The periodic boundary conditions essentially mean that the electron states exist in a large loop with a well in one part of it. In a finite system the states are discrete. The density of states is determined by the energy separation of these states, and how it changes when the well is added to the structure.

A state exists at a given energy whenever it is possible to construct a continuous, differentiable solution of the Schrödinger equation in all parts of space. In this problem, space breaks into three types of regions, bulklike regions, the interfaces that define the well at $x = \pm t/2$, and the point where periodic boundary conditions are applied, $x = \pm(L+t)/2$. Note that these two apparently different points are in fact the same point when periodic boundary conditions are applied. Any linear combination of the scattering states are continuous and differentiable in the bulk regions and at the interfaces, but in general not at the point where periodic boundary conditions are applied. States exist at energies at which there is a linear combination of scattering states that satisfy these conditions at this point.

All linear combinations of left and right going scat-

tering states with amplitudes A_L and A_R, respectively, are continuous and differentiable at the periodic boundary point if the scattered states reconstruct the incident states. This condition is satisfied when

$$A^R = A^R \Phi^{\mathrm{I},R}_{L/2} T^{W,R} \Phi^{\mathrm{I},R}_{L/2} + A^L \Phi^{\mathrm{I},L}_{-L/2} R^{W,L} \Phi^{\mathrm{I},R}_{L/2}, \quad \text{(A7)}$$

and

$$A^L = A^L \Phi^{\mathrm{I},L}_{-L/2} T^{W,L} \Phi^{\mathrm{I},L}_{-L/2} + A^R \Phi^{\mathrm{I},R}_{L/2} R^{W,R} \Phi^{\mathrm{I},L}_{-L/2}. \quad \text{(A8)}$$

These two equations can be written in a matrix form,

$$(A^R\ A^L) = (A^R\ A^L) \begin{pmatrix} \Phi^{\mathrm{I},R}_{L/2} T^{W,R} \Phi^{\mathrm{I},R}_{L/2} & \Phi^{\mathrm{I},R}_{L/2} R^{W,R} \Phi^{\mathrm{I},L}_{-L/2} \\ \Phi^{\mathrm{I},L}_{-L/2} R^{W,L} \Phi^{\mathrm{I},R}_{L/2} & \Phi^{\mathrm{I},L}_{-L/2} T^{W,L} \Phi^{\mathrm{I},L}_{-L/2} \end{pmatrix}. \quad \text{(A9)}$$

For a state to exist, there must be a solution with at least some A's not zero, which requires

$$\mathrm{Det} \begin{pmatrix} \Phi^{\mathrm{I},R}_{L/2} T^{W,R} \Phi^{\mathrm{I},R}_{L/2} - 1 & \Phi^{\mathrm{I},R}_{L/2} R^{W,R} \Phi^{\mathrm{I},L}_{-L/2} \\ \Phi^{\mathrm{I},L}_{-L/2} R^{W,L} \Phi^{\mathrm{I},R}_{L/2} & \Phi^{\mathrm{I},L}_{-L/2} T^{W,L} \Phi^{\mathrm{I},L}_{-L/2} - 1 \end{pmatrix} = 0. \quad \text{(A10)}$$

By making use of the properties of the Φ matrices as diagonal phase matrices, this condition can be simplified to

$$\mathrm{Det} \begin{pmatrix} \Phi^{\mathrm{I},R}_{L} T^{W,R} - 1 & \Phi^{\mathrm{I},R}_{L} R^{W,R} \\ \Phi^{\mathrm{I},L}_{-L} R^{W,L} & \Phi^{\mathrm{I},L}_{-L} T^{W,L} - 1 \end{pmatrix} = 0. \quad \text{(A11)}$$

This matrix is of the form

$$\mathrm{Det}\,[1 - S_{\mathrm{I}}(L) S_W(t)] = 0, \quad \text{(A12)}$$

where $S_W(t)$ is a reflection-transmission matrix for scattering from the well of thickness t, and $S_{\mathrm{I}}(L)$ is diagonal phase matrix describing propagation in the asymptotic regions of length L. Note that $S_W(t)$ includes the propagation through the well.

Based on flux conservation considerations, the eigenvalues of the matrix $S_{\mathrm{I}}(L) S_W(t)$ must all be pure phases. If an eigenvalue were not a phase, an initial set of amplitudes would all uniformly increase on a trip around the loop, increasing the flux through all of the states. There is a state on the loop whenever the determinant in Eq. (A12) is zero, which occurs whenever one of the eigenvalues of $S_{\mathrm{I}}(L) S_W(t)$ is one. Taking the determinant of this matrix gives the product of the eigenvalues, then taking the log gives the sum of the exponents of the phases. Whenever one of the exponents is equal to zero there is a state.

For any finite ring, the density of states is always a series of δ functions. In the limit of a large ring, the spacing of the δ functions is given by the energy derivative of exponents of the phases

$$[\Delta\epsilon]^{-1} = \frac{-i}{2\pi} \frac{d}{dE} [\ln[\mathrm{Det} S_{\mathrm{I}}(L) S_W(t)]]. \quad \text{(A13)}$$

If the δ functions are smeared over some finite energy resolution the density of states is then

$$n(E, L, t) = -i \frac{d}{dE} [\ln[\mathrm{Det} S_{\mathrm{I}}(L) S_W(t)]]. \quad \text{(A14)}$$

Using the the fact that a determinant of a product is the product of the determinants, and subtracting the bare density of states of materials I and II of length L and t, respectively, the change in the density of states is

$$\Delta n(E, t) = -i \frac{d}{dE} [\ln[\mathrm{Det} S_W(t) - \mathrm{Det} S_{\mathrm{II}}(t)]]. \quad \text{(A15)}$$

Since the propagation through the well, but not through the asymptotic regions, is included in $S_W(t)$, the final result subtracts the bare density of states of the former, but not the latter.

This result for the change in the density of states is quite general. It holds for any band structure in both of the materials. It also holds if the scattering matrix $S_W(t)$ is calculated including the contributions from the evanescent contributions to the scattering states. In fact, it holds if the scattering is calculated using the self-consistent potential that would result if the charge transfer due to the presence of the well was accounted for. Unfortunately, it needs to be calculated numerically in all but the simplest approximations. Below I discuss such approximations.

Using this general form for the change in the density of states, the change in energy as a function of thickness is

$$\frac{E(t)}{A} = \int_{\mathrm{IBZ}} \frac{d^2K}{(2\pi)^2} \int_{-\infty}^{E_F} \frac{dE}{2\pi} (E - E_F) \Delta n(E, \mathbf{K}, t), \quad \text{(A16)}$$

where the parallel momentum integration is over the interface Brillouin zone (IBZ), and the dependence of the change in the density of states on parallel momentum and thickness have been made explicit. Integrating the change in density of states by parts gives a form very reminiscent of integrating a phase shift as would be done for scattering from a central potential.

3. Symmetric one-band case

If there is only one band at a particular energy and both materials have a mirror plane symmetry perpendicular to the interface normal, then the left going and right going waves are mirror images of each other, the change in the density of states is particularly simple. The transmission and reflection matrices are just numbers and

commute with each other, and transmission across the well is the same from either direction $T^{W,L} = T^{W,R} = T^W$. In this case, the log of the determinant of the unitary transmission-reflection matrix is

$$\ln[\mathrm{Det}S] = [\ln(T^W - R^W) + \ln(T^W + R^W)]. \quad \text{(A17)}$$

Using the results for the well transmission and reflection amplitudes, the sum and difference are

$$T^W \pm R^W = \left[\mathrm{I} - R^{\mathrm{I,II,}L}R^{\mathrm{II,I,}R}\Phi_{2t}^{\mathrm{II,}R}\right]^{-1}\left\{T^{\mathrm{II,I,}L}\Phi_t^{\mathrm{II,}R}T^{\mathrm{I,II,}L} \pm R^{\mathrm{II,I,}L} \pm R^{\mathrm{I,II,}L}\Phi_{2t}^{\mathrm{II,}R}\left[-R^{\mathrm{II,I,}L}R^{\mathrm{II,I,}R} + T^{\mathrm{II,I,}L}T^{\mathrm{II,I,}R}\right]\right\}. \quad \text{(A18)}$$

For this case, the group velocities of the left and right going states have the same magnitude, and current conservation arguments require that $T^{\mathrm{II,I,}L}T^{\mathrm{II,I,}R} - R^{\mathrm{II,I,}L}R^{\mathrm{II,I,}R} = e^{i\phi}$. Symmetry requires that $R^{\mathrm{I,II,}L} = R^{\mathrm{II,I,}R}$, etc. If one reflection amplitude has the form $R^{\mathrm{I,II,}L} = -Re^{i\phi_L}$, the other must be $R^{\mathrm{I,II,}R} = Re^{i(\phi-\phi_L)}$. Using these relationships and pulling out front the phase factor due to propagation through the well gives

$$T^W \pm R^W = \Phi_t^{\mathrm{II,}R}\frac{[e^{i\phi} \pm Re^{i(\phi-\phi_L)}\Phi_{-t}^{\mathrm{II,}R}][1 \mp Re^{i\phi_L}\Phi_t^{\mathrm{II,}R}]}{[1 + Re^{i\phi_L}\Phi_t^{\mathrm{II,}R}][1 - Re^{i\phi_L}\Phi_t^{\mathrm{II,}R}]}. \quad \text{(A19)}$$

The phase factor out front gives the "bare" density of states for a thickness t of material II. One of the factors in the numerator cancels against one of those in the denominator giving

$$T^W \pm R^W = \Phi_t^{\mathrm{II,}R}e^{i\phi}\frac{[1 \pm Re^{-i\phi_L}\Phi_{-t}^{\mathrm{II,}R}]}{[1 \pm Re^{i\phi_L}\Phi_t^{\mathrm{II,}R}]}. \quad \text{(A20)}$$

Substituting this result into Eq. (A17) and Eq. (A15) and using the reflection amplitudes for the model shown in Fig. 2,

$$R = \frac{\sqrt{2m(E+V)} - \sqrt{2mE}}{\sqrt{2m(E+V)} + \sqrt{2mE}}, \quad \text{(A21)}$$

and phases $\phi = \phi_L = 0$ gives the change in the density of states plotted in Figs. 1 and 3.

The asymptotic form for the change in the density of states used in the asymptotic form for the oscillatory energy, Eq. (5), requires the log of the sum and difference of the transmission and reflection amplitudes:

$$\begin{aligned}
&\ln[T^W + R^W] + \ln[T^W - R^W] \\
&= 2ik_{\mathrm{II},R}t + 2i\phi + \ln[1 + Re^{-i\phi_L}\Phi_{-t}^{\mathrm{II,}R}] - \ln[1 + Re^{i\phi_L}\Phi_t^{\mathrm{II,}R}] + \ln[1 - Re^{-i\phi_L}\Phi_{-t}^{\mathrm{II,}R}] - \ln[1 - Re^{i\phi_L}\Phi_t^{\mathrm{II,}R}] \\
&= 2ik_{\mathrm{II},R}t + 2i\phi + 2\sum_{n=1}^{\infty}\frac{[Re^{-i\phi_L}\Phi_{-t}^{\mathrm{II,}R}]^{2n}}{2n} - 2\sum_{n=1}^{\infty}\frac{[Re^{i\phi_L}\Phi_t^{\mathrm{II,}R}]^{2n}}{2n} \\
&= 2ik_{\mathrm{II},R}t + 2i\phi - 2i\sum_{n=1}^{\infty}\frac{|R|^{2n}}{n}\sin(2n\phi_L + 2nk_{\mathrm{II},R}t).
\end{aligned} \quad \text{(A22)}$$

Note that in general there is a phase shift associated with reflection. This fact is not obvious in models based on a free-electron-like treatment of the transmission-reflection process. This phase shift contributes a nonoscillatory piece to all subsequent quantities, and a phase shift to the oscillatory energy.

The change in the energy due to the quantum well is

$$\Delta E = \int_{-\infty}^{E_F}\frac{dE}{2\pi}(E - E_F)(-i)\frac{d}{dE}\left(\ln[T^W + R^W] + \ln[T^W - R^W] - 2ik_{\mathrm{II},R}t\right). \quad \text{(A23)}$$

This expression can be integrated by parts to give

$$\Delta E = \int_{-\infty}^{E_F}\frac{dE}{2\pi}(-i)\left(\ln[T^W + R^W] + \ln[T^W - R^W] - 2ik_{\mathrm{II},R}t\right). \quad \text{(A24)}$$

Substituting in the result for the sum of the logs and canceling the contributions from the "bare" density of states gives

$$\Delta E = -\int_{-\infty}^{E_F} \frac{dE}{2\pi} 2 \sum_{1}^{\infty} \frac{R^{2n} \sin(2ntk + 2n\phi_L)}{n}. \quad \text{(A25)}$$

There is also a contribution to the energy from the phase shift associated with reflection, which has suppressed because it does not contribute to the oscillatory part. Taking the biggest term (assuming that the reflection probability is small) and changing the variables of integration gives

$$\Delta E = -\int^{k_F} \frac{dk}{2\pi} \frac{dE}{dk} 2R^2 \sin(2tk + 2\phi_L). \quad \text{(A26)}$$

This simple asymptotic form only holds when the reflection probability is much less than one. As the reflection probability approaches one from below more and more terms in the expansion of the logarithm become important. These higher-order terms change the shape, but not the period of the oscillatory component.

Assuming that the reflection probability is slowly varying and that the band dispersion is quadratic, this integral becomes

$$\begin{aligned} \Delta E &= -\frac{1}{\pi m} R^2 \int_0^{k_F} dk\, k \sin(2tk + 2\phi_L) \\ &= \frac{1}{\pi} R^2 \frac{k_F}{2m} \frac{1}{t} \left(\cos(2k_F t + 2\phi_L) - \frac{\sin(2k_F t + 2\phi_L) - \sin 2\phi_L}{2k_F t} \right). \end{aligned} \quad \text{(A27)}$$

Since the second term falls off as a higher power of the well thickness, only the first term is important in the asymptotic region, recovering the result given above in Eq. (5). This asymptotic form for the change in energy does not depend on the details of the dispersion. For a large enough well separation, the final form always holds, provided the bands are smoothly varying at the Fermi level.

4. General result for an isolated extremum

The results of the last two sections can be generalized to an isolated extrema associated with an arbitrary form for the Fermi surface. If there is more than one state in either of the materials at the Fermi energy the general result holds, Eq. (A15), but the approximate form derived below does not. Close to the Fermi surface, the dispersion can be written as

$$E = E_F + v_{iF}(k - k_{iF}) + \frac{1}{2m_{xi}}(k_x - k_{xi})^2 + \frac{1}{2m_{yi}}(k_y - k_{yi})^2, \quad \text{(A28)}$$

for one sheet with a similar expression indexed by j for the other sheet. Using these approximate forms, the difference in the z components of the wave vectors is

$$\Delta k_z = \Delta k_{ijF} + \frac{E - E_F}{v_{ijF}} - \frac{\alpha_{xij}}{2}(k_x - k_{xE})^2 - \frac{\alpha_{yij}}{2}(k_y - k_{yE})^2, \quad \text{(A29)}$$

where

$$\Delta k_{ijF} = (k_{iF} - k_{jF}) \quad \text{(A30)}$$

and

$$\frac{1}{v_{ijF}} = \frac{1}{v_{iF}} - \frac{1}{v_{jF}}, \quad \text{(A31)}$$

where v_{iF} and v_{jF} must have the opposite sign, and where

$$\alpha_{xij} = \frac{1}{m_{xi} v_{iF}} - \frac{1}{m_{xj} v_{jF}} \quad \text{(A32)}$$

is one over the radius of curvature of the Fermi surface in the x direction. Plugging this form for the difference wave vector in to the expression for the asymptotic oscillatory coupling,

$$\frac{\Delta E(t)}{A} = -2 \int_{-\infty}^{E_F} \frac{dE}{2\pi} \int \frac{dk_x}{2\pi} \int \frac{dk_y}{2\pi} R^2 \sin(t\Delta k_z + 2\phi_L), \quad \text{(A33)}$$

and assuming that the reflection probability is independent of the wave vector gives

$$\frac{\Delta E_\infty(t)}{A} = -2R^2 \int_{-\infty}^{E_F} \frac{dE}{2\pi} \int_{-\infty}^{\infty} \frac{dk_x}{2\pi} \int_{-\infty}^{\infty} \frac{dk_y}{2\pi} \sin\left[t\left((k_{iF} - k_{jF}) + \frac{E - E_F}{v_{ijF}} + \frac{\alpha_{xij}}{2}(k_x - k_{xE})^2 + \frac{\alpha_{yij}}{2}(k_y - k_{yE})^2 \right) + 2\phi_L \right]. \tag{A34}$$

First integrating over energy,

$$\frac{\Delta E_\infty(t)}{A} = 2R^2 \frac{v_{ijF}}{2\pi t} \int_{-\infty}^{\infty} \frac{dk_x}{2\pi} \int_{-\infty}^{\infty} \frac{dk_y}{2\pi} \cos\left[t(k_{iF} - k_{jF}) + 2\phi_L + t\alpha_{xij}(k_x - k_{xE})^2 + t\alpha_{yij}(k_y - k_{yE})^2 \right]. \tag{A35}$$

To do the integrals over parallel momentum, expand the cosine factor using multiple angle formulas, and do the integrations of the form

$$\int_{-\infty}^{\infty} dx \cos(ax^2) = \sqrt{\frac{\pi}{2|a|}}$$
$$\int_{-\infty}^{\infty} dx \sin(ax^2) = \mathrm{sgn}[a]\sqrt{\frac{\pi}{2|a|}}. \tag{A36}$$

The result is

$$\frac{\Delta E_\infty(t)}{A} = -\frac{|R|^2}{2\pi^2} v_{ijF} \sqrt{\frac{1}{|\alpha_{xij}\alpha_{yij}|}} \frac{1}{t^2} \left[-\cos(t\Delta k_{ijF} + 2\phi_L) \frac{1 - \mathrm{sgn}[\alpha_{xij}]\mathrm{sgn}[\alpha_{yij}]}{2} + \sin(t\Delta k_{ijF} + 2\phi_L) \frac{\mathrm{sgn}[\alpha_{xij}] + \mathrm{sgn}[\alpha_{yij}]}{2} \right]. \tag{A37}$$

The term in square brackets gives the phase shift due to the type of extrema. If α_{xij} and α_{yij} have opposite signs, the extremum is a saddle point, and there is no phase shift due to the integration over parallel momentum. If they have the same sign, there is a phase shift of $\pm\pi/2$, depending on whether the extremum is a maximum or a minimum. Simplifying gives the final result

$$\frac{\Delta E_\infty(t)}{A} = \frac{1}{2\pi^2} v_{ijF} \kappa_{ijF} R^2 \frac{1}{t^2} \cos\left(t\Delta k_{ijF} + \phi'\right). \tag{A38}$$

The phase shift ϕ' includes not only the usual phase shift due to the different types of extrema, but also the phase shift due to reflection from each of the well boundaries.

[1] P. Grünberg *et al.*, Phys. Rev. Lett. **57**, 2442 (1986).
[2] S. S. P. Parkin, N. More, and K. P. Roche, Phys. Rev. Lett. **64**, 2304 (1990).
[3] M. N. Baibich *et al.*, Phys. Rev. Lett. **61**, 2472 (1988).
[4] G. Binasch, P. Grünberg, F. Saurenbach, and W. Zinn, Phys. Rev. B **39**, 4828 (1989).
[5] L. M. Falicov, Phys. Today **45**, 46 (1992).
[6] J. Unguris, R. J. Celotta, and D. T. Pierce, Phys. Rev. Lett. **67**, 140 (1991).
[7] S. Demokritov, J. A. Wolf, and P. Grünberg, Europhys. Lett. **15**, 881 (1991).
[8] S. T. Purcell *et al.*, Phys. Rev. Lett. **67**, 903 (1991).
[9] Z. Q. Qiu, J. Pearson, A. Berger, and S. D. Bader, Phys. Rev. Lett. **68**, 1398 (1992).
[10] M. T. Johnson *et al.*, Phys. Rev. Lett. **68**, 2688 (1992).
[11] M. T. Johnson *et al.*, Phys. Rev. Lett. **69**, 969 (1992).
[12] Z. Q. Qiu, J. Pearson, and S. D. Bader, Phys. Rev. B **46**, 8659 (1992).
[13] A. Cebollada *et al.*, J. Magn. Magn. Mater. **103**, L221 (1992).
[14] W. R. Bennett, W. Schwarzacher, and W. Egelhoff, J. Appl. Phys. **70**, 5881 (1991).
[15] Z. Celinski and B. Heinrich, J. Magn. Magn. Mater. **99**, L25 (1991).
[16] J. Unguris, R. J. Celotta, and D. T. Pierce, J. Magn. Magn. Mater. (to be published).
[17] A. Fuss, S. Demokritov, P. Grünberg, and W. Zinn, J. Magn. Magn. Mater. **103**, L221 (1992).
[18] K. Ounadjela *et al.*, J. Magn. Magn. Mater. **104-107**, 1896 (1992).
[19] S. S. P. Parkin, Phys. Rev. Lett. **67**, 3598 (1991).
[20] S. S. P. Parkin, R. Bhadra, and K. P. Roche, Phys. Rev.

Lett. **66**, 2152 (1991).
[21] F. Petroff *et al.*, Phys. Rev. B **44**, 5355 (1991).
[22] S. Honda, T. Mimura, S. Ohmoto, and M. Nawate, IEEE Trans. Mag. **28**, 2745 (1992).
[23] D. H. Mosca *et al.*, J. Magn. Magn. Mater. **94**, L1 (1991).
[24] M. E. Tomlinson, R. J. Pollard, D. G. Lord, and P. J. Grundy, J. Magn. Magn. Mater. **111**, 79 (1992).
[25] J. Fassbender *et al.*, Phys. Rev. B **46**, 5810 (1992).
[26] Y. Huai and R. W. Cochrane, J. Appl. Phys. **72**, 2523 (1992).
[27] P. J. H. Bloeman, W. J. M. de Jonge, and R. Coehoorn, J. Magn. Magn. Mater. **121**, 306 (1993).
[28] J. E. Mattson, C. H. Sowers, A. Berger, and S. D. Bader, Phys. Rev. Lett. **68**, 3252 (1992).
[29] M. E. Brubaker, J. E. Mattson, C. H. Sowers, and S. D. Bader, Appl. Phys. Lett. **58**, 2306 (1991).
[30] F. J. Himpsel, Phys. Rev. B **44**, 5966 (1991).
[31] J. E. Ortega and F. J. Himpsel, Phys. Rev. Lett. **69**, 844 (1992).
[32] J. E. Ortega, F. J. Himpsel, G. J. Mankey, and R. F. Willis, Phys. Rev. B **47**, 1540 (1993).
[33] N. B. Brookes, Y. Chang, and P. D. Johnson, Phys. Rev. Lett. **67**, 354 (1991).
[34] P. D. Johnson, N. B. Brookes, Y. Chang, and K. Garrison (unpublished).
[35] D. M. Edwards, J. Mathon, R. B. Muniz, and M. S. Phan, Phys. Rev. Lett. **67**, 493 (1991).
[36] P. Bruno and C. Chappert, Phys. Rev. Lett. **67**, 1602 (1991).
[37] P. Bruno, J. Magn. Magn. Mater. **121**, 248 (1993).
[38] D. M. Deaven, D. S. Rokhsar, and M. Johnson, Phys. Rev. B **44**, 5977 (1991).
[39] R. Coehoorn, Phys. Rev. B **44**, 9331 (1991).
[40] C. Chappert and J. P. Renard, Europhys. Lett. **15**, 553 (1991).
[41] F. Herman and R. Schrieffer, Phys. Rev. B **46**, 5806 (1992).
[42] L. F. Mattheis and D. R. Hamman, Phys. Rev. B **33**, 823 (1986).
[43] D. A. Papaconstantopoulos, *Handbook of the Band Structure of Elemental Solids* (Plenum, New York, 1986).
[44] M. D. Stiles (unpublished).
[45] W. F. Egelhoff and M. T. Kief, Phys. Rev. B **45**, 7795 (1992).
[46] P. J. H. Bloemen, M. T. Johnson, J. aan de Stegge, and W. J. M. de Jonge, J. Magn. Magn. Mater. **116**, L315 (1992).
[47] S. T. Purcell *et al.*, Phys. Rev. B **45**, 13064 (1992).
[48] Y. Wang, P. M. Levy, and J. L. Fry, Phys. Rev. Lett. **65**, 2732 (1990).
[49] D. Stoeffler and F. Gautier, Phys. Rev. B **44**, 10389 (1991).
[50] K. B. Hathaway, in *Ultrathin Magnetic Structures*, edited by B. Heinreich and A. Bland (Springer-Verlag, in press).
[51] J. Barnas, J. Magn. Magn. Mater. **111**, L215 (1992).
[52] R. P. Erickson, K. B. Hathaway, and J. R. Cullen, Phys. Rev. B **47**, 2626 (1993).
[53] K. B. Hathaway and J. R. Cullen, J. Magn. Magn. Mater. **104-107**, 1840 (1992).
[54] J. R. Cullen and K. B. Hathaway, J. Appl. Phys. **70**, 5879 (1991).
[55] D. M. Edwards, J. Mathon, R. B. Muniz, and M. S. Phan, J. Phys.: Condens. Matter **3**, 4941 (1991).
[56] D. M. Edwards, R. B. Muniz, and J. Mathon, Phys. Scr. **T45**, 91 (1992).
[57] J. Mathon, M. Villeret, and D. M. Edwards, J. Phys.: Condens. Matter **4**, 9873 (1992).
[58] J. Mathon, D. M. Edwards, R. B. Muniz, and M. S. Phan, J. Magn. Magn. Mater. **104-107**, 1721 (1992).
[59] M. S. Phan, J. Mathon, D. M. Edwards, and R. B. Muniz, J. Magn. Magn. Mater. **104-107**, 1876 (1992).
[60] C. Lacroix, B. Dieny, J. P. Gavigan, and D. Givord, Thin Solid Films **193-194**, 877 (1990).
[61] C. Lacroix and J. P. Gavigan, J. Magn. Magn. Mater. **93**, 413 (1991).
[62] Y. Wang, P. M. Levy, and J. L. Fry, J. Magn. Magn. Mater. **93**, 395 (1991).
[63] J. L. Fry, E. C. Ethridge, P. M. Levy, and Y. Wang, J. Appl. Phys. **69**, 4780 (1991).
[64] Z.-P. Shi, P. M. Levy, and J. L. Fry, Phys. Rev. Lett. **69**, 3678 (1992).
[65] P. Bruno, J. Magn. Magn. Mater. **116**, L13 (1992).
[66] P. Bruno and C. Chappert, Phys. Rev. B **46**, 261 (1992).
[67] D. Stoeffler and F. Gautier, Prog. Theor. Phys. Suppl. **101**, 139 (1990).
[68] D. Stoeffler, K. Ounadjela, and F. Gautier, J. Magn. Magn. Mater. **93**, 386 (1991).
[69] A. Vega *et al.*, J. Appl. Phys. **69**, 4544 (1991).
[70] H. Hasegawa, Phys. Rev. B **42**, 2368 (1990).
[71] H. Hasegawa, Phys. Rev. B **43**, 10803 (1991).
[72] F. Herman, J. Sticht, and M. Van Schilfgaarde, J. Appl. Phys. **69**, 4783 (1991).
[73] K. Ounadjela *et al.*, Europhys. Lett. **15**, 875 (1991).
[74] J.-H. Xu and A. J. Freeman, Phys. Rev. B **47**, 165 (1993).
[75] S. Mirbt, H. L. Skriver, M. Aldén, and B. Johansson (unpublished).